UTILIZING DISTRIBUTED TEMPERATURE AND PRESSURE DATA TO EVALUATE THE PRODUCTION DISTRIBUTION IN MULTILATERAL WELLS

A Thesis

by

RASHAD MADEES K. AL ZAHRANI

Submitted to the Office of Graduate Studies of
Texas A&M University
in partial fulfillment of the requirements for the degree of

MASTER OF SCIENCE

May 2011

Major Subject: Petroleum Engineering

Utilizing Distributed Temperature and Pressure Data to Evaluate The Production Distribution in Multilateral Wells

UTILIZING DISTRIBUTED TEMPERATURE AND PRESSURE DATA TO EVALUATE THE PRODUCTION DISTRIBUTION IN MULTILATERAL WELLS

A Thesis

by

RASHAD MADEES K. AL ZAHRANI

Submitted to the Office of Graduate Studies of
Texas A&M University
in partial fulfillment of the requirements for the degree of

MASTER OF SCIENCE

Approved by:

Chair of Committee, Ding Zhu
Committee Members, Daniel Hill
Wolfgang Bangerth
Head of Department, Steven Holditch

May 2011

Major Subject: Petroleum Engineering

ABSTRACT

Utilizing Distributed Temperature and Pressure Data To Evaluate The Production Distribution in Multilateral Wells. (May 2011)

Rashad Madees K. Al-Zahrani, B.S., Texas A&M University

Chair of Advisory Committee: Dr. Ding Zhu

One of the issues with multilateral wells is determining the contribution of each lateral to the total production that is measured at the surface. Also, if water is detected at the surface or if the multilateral well performance declines, then it is difficult to identify which lateral or laterals are causing the production decline.

One way to estimate the contribution from each lateral is to run production Logging Tools (PLT). Unfortunately, PLT jobs are expensive, time-consuming, labor-intensive and involve operational risks. An alternative way to measure the production from each lateral is to use Distributed Temperature Sensing (DTS) technology. Recent advances in DTS technology enable measuring the temperature profile in horizontal wells with high precision and resolution. The changes in the temperature profile are successfully used to calculate the production profile in horizontal wells.

In this research, we develop a computer program that uses a multilateral well model to calculate the pressure and temperature profile in the motherbore. The results

help understand the temperature and pressure behaviors in multilateral wells that are crucial in designing and optimizing DTS installations. Also, this model can be coupled with an inversion model that can use the measured temperature and pressure profile to calculate the production from each lateral.

Our model shows that changing the permeability or the water cut produced from one lateral results in a clear signature in the motherbore temperature profile that can be measured with DTS technology. However, varying the length of one of the lateral did not seem to impact the temperature profile in the motherbore. For future work, this research recommends developing a numerical reservoir model that would enable studying the effect of lateral inference and reservoir heterogeneity. Also recommended is developing an inversion model that can be used to validate our model using field data.

DEDICATION

To a casual observer, this thesis might appear to be a solitary work. However, to complete such a journey requires a great deal of support, encouragement and discipline, and I am indebted to my father and mother for supporting me all the way. There is nothing in the world I can do to pay them back but I know my academic and professional success gives them the greatest satisfaction.

I am also so grateful to my beautiful wife, Haifa, who completed her M.S. in economics this semester. Despite being so busy, she still managed to be the lovely and supportive wife I have always known. Also, I am so thankful to my brother and sister for their prayers and support. Last but not least, I always thank God, Allah, for blessing me with my cute, funny and energetic daughter, Lamar.

ACKNOWLEDGEMENTS

I am heartily thankful to my advisor, Dr. Ding Zhu, for her support and guidance throughout this research, and for her trust in my abilities and interests. My special thanks to her for being so patient in teaching me such an involved topic that transformed my understanding of Distributed Temperature Sensing (DTS) technology and its application in wellbore flow modeling.

I am also so grateful to Dr. A. Daniel Hill and Dr. Wolfgang Bangerth for their willingness to serve as members on this thesis committee and for being always available to help and comment on my work as needed.

Finally, many thanks to the great Saudi community in College Station, TX for making our stay here so enjoyable. Among my Saudi colleagues, I would like to thank Jassim Al-Mullah, Bandar Al-Khamis, Abduallah Al-Yami, and Abdullwahab Al-Ghamdi, for being so nice and supportive during my stay here in the United States.

NOMENCLATURE

Symbol	Description
$\hat{\rho}$	Specific density
μ	Viscosity
C	Casing
cem	Cement
Cp	Specific heat capacity
CV	Parameter used in the calculation of pressure drop across ICV's that accounts for how the pressure changes with the changing the opening of the valve
D	Diameter
D*	Dimensionless diameter
DTS	Distributed temperature sensing
F	Friction factor
f_0	Friction factor without inflow effect
G	Acceleration of gravity, 9.8 m/s
G	Gas
H	Enthalpy
I	A certain phase
I_{ani}	Anistropy ratio
ICV	Inflow Control Valve
In	Inflow
J	A certain segment

Symbol	Description
K	Permeability
k_H	Horizontal permeability
K_{JT}	Joule-Thompson coefficient
K_T	Formation conductivity
Ku	Kutateladze number
k_V	Vertical permeability
L	Length
L	Liquid
ML	Multilateral
N	Maximum number of segments in the wellbore
N_{Re}	Reynolds number in pipe
$N_{Re,w}$	The inflow Reynolds number
O	Oil
P	Pressure
Pr	Prandtl number
Q	Flow rate
Q	Heat Flux
R	Indicates the radial direction
r_w	Wellbore radius
T	Temperature
Tp	Two-phase

Symbol	Description
U	Overall heat transfer coefficient in a pipe; not perforated
$U_{overall}$	Overall heat transfer coefficient including inflow effect
V	Velocity
W	Water
X	Liquid fraction
X	Indicates the direction along the pipe
y	Fraction of a phase in a fluid
yb	Half the width of the box-shaped reservoir in Furui's model
Λ	Gas fraction
Λ	Fraction of segment that is open area
P	Density
Σ	Surface tension
T	Stress tensor
Φ	Combined stress tensor
Θ	Inclination angle

TABLE OF CONTENTS

Page

Page

LIST OF FIGURES

Page

Page

LIST OF TABLES

Page

1. INTRODUCTION

1.1 Background

Advances in drilling and completion technologies have enabled drilling more complex well structures to increase productivity in a cost-effective manner. Horizontal wells have been utilized to increase the reservoir contact area and thus increasing the total production rate and improving the reservoir sweep efficiency. Also, horizontal wells can be used to delay water encroachment by drilling at the top of productive formations so to stay as far as possible from the water table. In addition, multilateral wells have enabled accessing multiple formations from the same well while reducing drilling foot print. One of the milestones in the application of multilateral well technology, as Al-Kaabi (2008) indicated, is what Saudi Aramco have accomplished in developing Haradh Inc-3, a subfield of the Ghawar field. The field was developed with thirty two multilateral wells, predominantly trilateral wells, to achieve a target rate of 300 MBPD. This development scheme coupled with the inflow control valves (ICV's) enabled reducing the number of wells required for the target production rate as well as the development cost per barrel as shown in **Fig. 1.1**, by Al-Kaabi (2008).

This thesis follows the style of *SPE Production & Operations.*

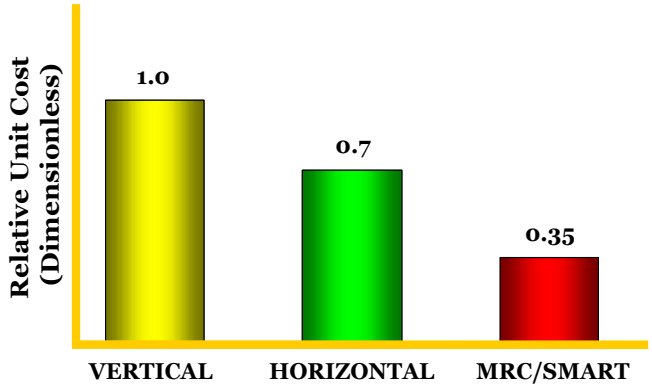

Fig. 1.1: Relative Development Unit Well Costs for HRDH Inc-3; Costs are Relative to Vertical Wells in $/BPD.

Although they were intended as means of allocating hydrocarbons, temperature logs were applied to analyze well production or injection profiles. Hill (1990) implied that the applications focused on vertical wells, were more qualitative in nature and were aimed at identifying anomalous behaviors in temperature profiles. These applications included identifying gas entry zones, casing leaks and lost circulation zones. However, in horizontal or near horizontal wells, Yoshioka (2007) indicated that the geothermal gradient does not play an important role and that the temperature variation along the wellbore is caused by subtle effects mainly; the fluid expansion and the viscous dissipation effects. This small temperature change can be used to interpret openhole flow profile.

Another challenge for horizontal wells is that the temperature variation is estimated to be in the order of several degrees as reported by Yoshioka (2007) and Dawkrajai (2006). Such difference cannot be detected with the conventional temperature sensors run in ordinary temperature logs. However, Fiber-optic distributed temperature sensing (DTS) technology enables detecting temperature changes in the order of 0.01^{o}C

with continuous monitoring ability for up to 60 km and with a short updating time of 10 seconds (Sensornet 2009). Also, DTS technology provides many advantages in monitoring and optimizing well performance and integrity. The DTS is provided continuously, real-time and requires no wellbore intervention. This provides cost-effective and safe alternative to the conventional PLT jobs. Moreover, DTS technology includes surface readout units that can be easily integrated into an existing network of transferring and storing data which can be integrated in future development of intelligent fields.

The increasing field installations of DTS technology show the increasing confidence in the technology as well as the versatile applications. Nath et al. (2006) cited successful application of DTS technology in Indonesia. The operator was able to monitor the water breakthrough in a horizontal well and determine the pump- and motor-operating conditions of the installed Electrical Submersible Pump (ESP). Also, this information enabled the optimization of ESP installations in the area. Glasbergen et al. (2009) presented a field case for a method to quantify the diversion effect for acid jobs. They used a tracer slug concept and interpreted the temperature profile before and after the treatment to infer the effectiveness of the diversion.

In Saudi Arabia, Hembling et al. (2010) reported several field applications of a DTS system installed on a Multilateral well. The well was equipped with ICV's to control each lateral individually. The applications included the confirmation of ICV operations and confirmation that the subsurface sliding door, SSD, has closed. Also and

more importantly, the effect of inflow from each lateral was seen on the temperature log as spikes of increased temperature.

1.2 Literature Review

Hill (1990) implied that most of the earlier work using temperature logging was on vertical wells with the focus on anomalies in the temperature profile because of gas entry or on monitoring well integrity to identify casing leaks or lost circulation zones. Also, the applications tended to be more qualitative in nature, identifying the place of the anomaly, and less quantitative; i.e. determining the actual rates.

Dawkrajai (2006) studied the feasibility of using DTS data to infer production profile and developed several synthetic cases to understand the range for temperature changes caused by flow rates. He developed a numerical reservoir temperature and pressure models coupled with multiphase wellbore flow model and solve the model iteratively. He concluded that the two main contributors to the temperature profile in the case of horizontal wells are the fluid thermal expansion and the viscous dissipation. He also concluded that the wellbore temperature derivate showed a remarkable change when different phase enters the wellbore especially for gas inflow zones. He showed that oil and water enters the wellbore 3-4 ^{o}F higher than the geothermal but gas enters the wellbore at 5-6 ^{o}F lower than the geothermal temperature. However, Dawkrajai indicated that no –inflow zones were difficult to identify using DTS temperature data.

Yoshioka's work (2007) paralleled that of Dawkrajai with the difference being in the reservoir model. Yoshioka used the reservoir pressure model developed by Furui et

al. (2003). Furui assumed steady-state, box-shaped reservoir with the well fully penetrating the entire reservoir and flow perpendicular to the wellbore and with no flow in the axial direction. He divided the reservoir into two regions according to the streamline shape; the linear region from the boundaries to a certain distance from the wellbore and a radial region extending from the wellbore wall to a certain distance into the reservoir. Combining the solutions in both regions, He solved for the total rate and showed a good agreement with reservoir simulation results. Following the same approach, Yoshioka assumed steady-state conditions and developed analytical reservoir temperature models for the linear and radial regions. He then combined both solutions to come up with final solution for the temperature profile in the reservoir. From the reservoir model, Yoshioka concluded that the temperature profile increased gradually in the linear region and rapidly in the radial region. Also, he was able to simplify the reservoir temperature solution by ignoring the heat conduction term in the linear region without compromising on the accuracy of the solution. Additionally, Yoshioka developed an inversion model and presented its applicability using production log data on a horizontal well in the North Sea in which he was able to match the pressure and temperature profiles and successfully estimate the inflow rates.

Sui (2009) detailed a method of using DTS transient temperature and pressure data to characterize properties of multilayered reservoirs in vertical wells. Her findings showed that the temperature data can be used to determine the radius of damage which cannot be determined from the pressure data alone.

Hembling et al. (2008) presented a field installation of a DTS system in a multilateral well. The temperature profile measured enabled Saudi Aramco to confirm that the downhole inflow control valves (ICV) are operating and to monitoring the displacement of diesel in the annulus through the Selective Shutting Device (SSD). After six weeks, the well was put on production and the temperature profile clearly showed the inflow at the laterals since the fluid from the laterals entered the motherbore at a higher temperature than the fluid in the motherbore.

To develop models to account for small temperature and pressure changes, a detailed wellbore model has to be developed. Numerous wellbore multiphase flow models are present in the petroleum engineering literature, Shoham (2006), including the drift-flux and mechanistic modeling. The drift-flux model is easier to implement in simulation work and is the one commonly used in commercial reservoir simulators. Shi et al. (2005) conducted extensive experimental work to determine the appropriate values for the drift-flux model parameters for water/gas, oil/water and oil/water/gas systems. Their calculated parameter values show excellent agreement with the experimental data. Ouyang (1998) developed a homogeneous model to calculate the pressure drop in horizontal wells for the gas/liquid system. The liquid phase treated oil and water as a homogeneous phase using mixture properties that are weighted based on volumetric ratios. Their model accounts for the inflow effect and shows a good agreement with the experimental data.

1.3 Research Objectives

The objective of this research is to develop a theoretical model and a computer program that performs forward calculation of the temperature and pressure profiles in multilateral wells. Given the reservoir conditions and well configuration, the model will generate a pressure and temperature profile in the motherobore which is the main bore connecting with the laterals. The results will help understand the temperature and pressure behavior in multilateral wells which is crucial in designing and optimizing future DTS installations. Moreover, this program can be coupled with an inversion model in which the production from each lateral is calculated based on the measured temperature and pressure profiles. This will have great utility to field-operating companies when performing production testing jobs as the contribution from each lateral can be determined real-time. Since the DTS system is permanently installed, continuous production profile will be generated that will help in future optimizations and enable detecting water or gas breakthrough.

To better understand the problem and the assumptions made in developing this model, a brief description of the system installation is needed. This study will use specific multilateral well configurations. We will use trilateral or dual wells normally drilled in the same formation and at almost the same elevation. Sometimes, a small inclination exists. **Fig. 1.2** and **Fig. 1.3** show diagrams of a typical installation. The production tubing is run in the motherbore and is bullnosed; tubing is closed at the end. Therefore, all the flow comes through the ICV and production from all laterals is comingled in the motherbore.

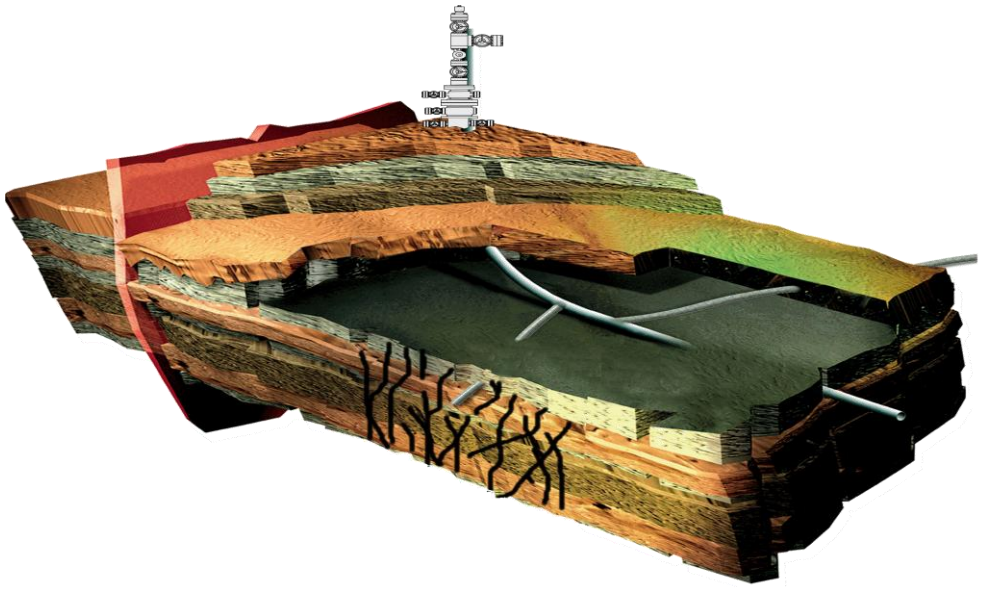

Fig. 1.2: A Typical Multilateral Well Drilled in Saudi Arabia; This is a Trilateral Well.

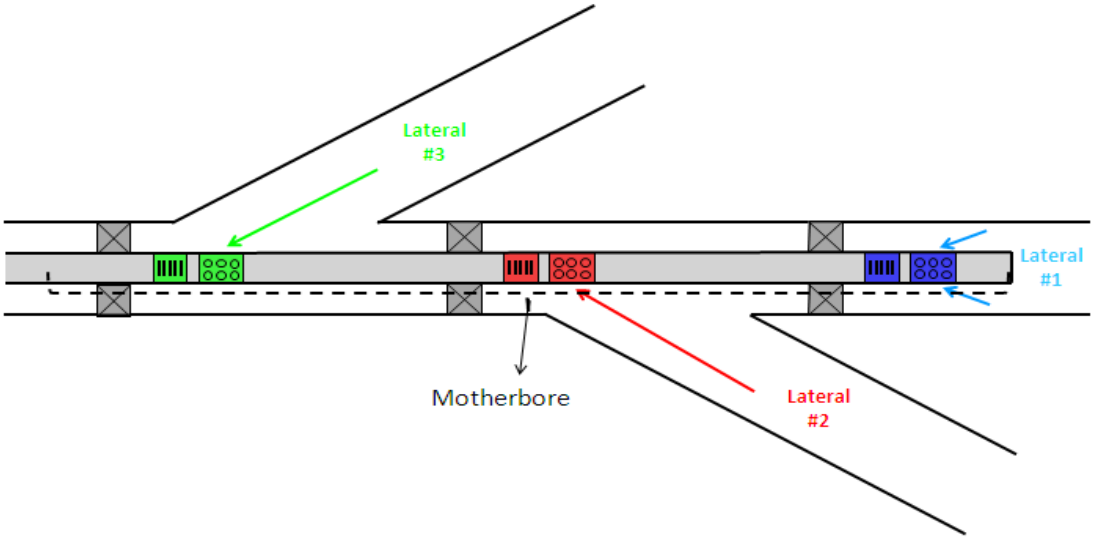

Fig. 1.3: Top-View of a Trilateral Well Showing the Tubing, Packers and ICV Installations.

The DTS and pressure sensors are installed in the interior of the motherbore pipe. The fiber-optic cables are clapped on the tubing and run from the toe of the well, total depth, all the way to the wellhead. The data is transferred and stored in a surface readout unit where it can be retrieved for further analysis. This feature makes DTS technology more compatible with intelligent field applications where monitoring and control is envisioned to be performed real-time and remotely with minimum field personnel involvement on the wellsite.

1.4 Organization of the Thesis

The second Section of this thesis will discuss the development of the wellbore model. Section 2.1 will describe the geometry of the model considered and the assumptions made. Attempts will be made to explain the validity and the value of each assumption. In Section 2.2, we will derive the mass balance equations for the single and multiphase flow conditions. Section 2.3 will present the derivation of the momentum balance equations for single and multiphase flow conditions which determine the pressure drop in the wellbore. In Section 2.4, we derive the energy balance equation for the single and multiphase flows which describe the temperature profile in the wellbore. All the equations will be written in a discrete form using finite difference approximation as this will be the form used in the actual model. Section 3 will discuss the reservoir model; both the pressure and temperature models along with the important assumptions made. The details of the derivation will not be shown as the model has been derived several times before by Furui (2003), Dawkrajai (2006) and Yoshioka (2007) and we use the exact same formulation. After that, Section 4 will present the coupling of wellbore

and reservoir models to generate the pressure and temperature profiles. In this Section, we will detail all the steps and assumptions made in our model. In Section 5, we will start by examining results for horizontal wells. These results will help us analyze and interpret our results for multilateral wells. After that, we will study the effect of varying several parameters like permeability, wellbore length and water cut on temperature profiles in multilateral wells. Finally, Section 6 will present the research conclusions and recommendations.

2. WELLBORE MODEL

2.1 Introduction

Multilateral wells consistent of two or more horizontal laterals that are tied to a main bore, the motherbore, in which the production is comingled, as shown by Fig 1.2. Therefore, the first step in developing a multilateral well model is to derive the equations used for each of the horizontal laterals. In this Section, we derive the wellbore model. Our approach is to develop the mass balance, momentum balance and energy balance in discrete forms using finite-difference method. Because of the different flow phenomena between single and multiphase flows, two sets of equations will be developed for each case; i.e. for the single phase and multiphase flow cases. The finite difference forms will be used for the coupled model presented in Section 4. The wellbore model derivation parallels Yoshioka's (2007) derivation but with some modifications on the notations, assumptions and correlations used.

Fig. 2.1 shows a general diagram of one lateral along with a representative segment to explain some geometrical variables and the frame of reference chosen. Since wellbores are cylindrical shaped, it makes a perfect sense to choose cylindrical coordinates for the derivation. There are two components that will be considered in our derivation; the axial and radial components. The axial component is always much larger than the radial component therefore we will make the assumption that the radial component only exists at the wall of the pipe. Mathematically, this is represented by Eq. 2.1.

$$v = \begin{pmatrix} v_x \\ v_r \\ v_\theta \end{pmatrix} = \begin{cases} \begin{pmatrix} v_x \\ 0 \\ 0 \end{pmatrix} \; Anywhere\ in\ the\ pipe \\ \begin{pmatrix} 0 \\ v_{in} \\ 0 \end{pmatrix} \; @\, r = r_w \end{cases} \qquad \ldots (2.1)$$

The radial distance "r_w" represents the wellbore radius. Also, wellbores can have different types of completions ranging from openhole to casing and perforated. Fig. 2.1 shows case of a perforated segment and to account for the fact that part of the segment can be closed and not open for flow, we introduce the variable (λ) defined as follows;

$$\lambda = \frac{Open\ surface\ area\ of\ the\ pipe}{Total\ surface\ area\ of\ the\ pipe} \qquad \ldots (2.2)$$

The value of this parameter is one for openhole completion and is equivalent to the perforation density for a perforated segment. The inflow velocity ($\boldsymbol{v_{in}}$) is calculated by Eq. 2.3 using the inflow rate which is determined by Furui's equation which will be explained in Section 3.

$$v_{j,in} = \frac{Q_{j,in}}{2\pi R \lambda \Delta x} \qquad \ldots (2.3)$$

where "j" represents a certain segment.

Throughout our derivation for the wellbore model, we will assume that the well has been flowing for a period of time long enough to achieve a steady-state conditions. Moreover, in the problem we are investigating, the pressure and temperature variations are not significant since all the laterals in a ML well are drilled in the same formation at almost the same elevations. Therefore fluid properties are assumed to be constants and

will be supplied at the average pressure and temperature expected in well modeled. Additionally, pressures are assumed to be above the bubble point pressure so that no gas is liberated out of the oil phase.

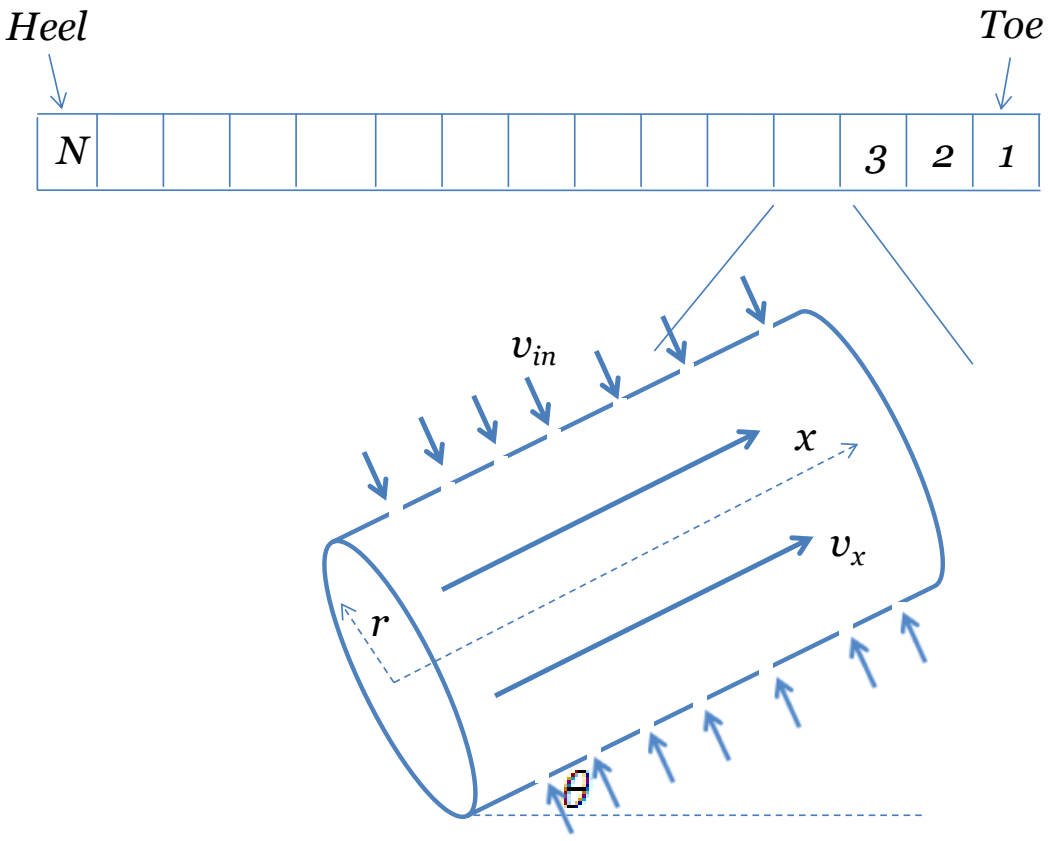

Fig. 2.1: A Diagram Showing Lateral's Segmentation Scheme and the Frame of Reference.

2.2 Mass Balance

2.2.1 Single Phase Flow

In steady-state conditions, conservation of mass states that the rate of mass entering the system must equal to the rate of mass exiting. Mathematically this relationship is represented by Eq. 2.4, Eq. 2.5 and Eq. 2.6.

$$(Rate\ of\ mass\ in) = (Rate\ of\ mass\ out) \quad (2.4)$$

$$(Rate\ of\ Mass\ in) = \pi R^2(\rho v_x)|_x + 2\pi R \Delta x \lambda(\rho v_{in}) \quad (2.5)$$

$$(Rate\ of\ Mass\ out) = \pi R^2(\rho v_x)|_{x+\Delta x} \quad (2.6)$$

Substituting Eq. 2.5 and Eq. 2.6 into Eq. 2.4 and cancelling out the density since it is assumed to be constant gives

$$\pi {r_w}^2(v_x)|_x + 2\pi r_w \Delta x \lambda(v_{in}) = \pi {r_w}^2(v_x)|_{x+\Delta x} \quad (2.7)$$

Rearranging Eq. 2.7 and dividing by $(\pi {r_w}^2 \Delta x)$ gives

$$\frac{(v_x)|_{x+\Delta x} - (v_x)|_x}{\Delta x} = \frac{2\lambda(v_{in}).}{r_w} \quad (2.8)$$

Assuming that the wellbore is divided into segments and using the subscript, j, to refer to a specific segment, Eq. 2.8 can be written in its final form as shown below.

$$v_{x_j} = v_{x_{j-1}} + \frac{2\Delta x \lambda(v_{in}).}{r_w} \quad (2.9)$$

2.2.2 Multiphase Flow

For multiphase flow, we will use the subscript "i" to indicate a certain phase and the subscript "j" to indicate a certain segment. We apply Eq. 2.5 and Eq. 2.6 for each phase as follows

$$(Rate\ of\ Mass\ in) = \pi {r_w}^2 \left(y_i \rho_i v_{i,x}\right)|_x + 2\pi r_w \Delta x \lambda \left(\rho_i v_{in,i}\right)|_{r=rw} \dots\dots\dots\dots\dots (2.10)$$

$$(Rate\ of\ Mass\ out) = \pi {r_w}^2 \left(y_i \rho_i v_{i,x}\right)|_{x+\Delta x} \dots\dots\dots\dots\dots\dots\dots\dots\dots\dots\dots\dots (2.11)$$

Rate of mass input should equal to the rate of mass output, therefore we set Eq. (2.10) and Eq. (2.11) equal, we obtain Eq. (2.12)

$$\pi {r_w}^2 \left(y_i \rho_i v_{i,x}\right)|_x + 2\pi r_w \Delta x \lambda \left(\rho_i v_{i,in}\right)|_{r=rw} = \pi {r_w}^2 \left(y_i \rho_i v_{i,x}\right)|_{x+\Delta x} \dots\dots\dots\dots\dots (2.12)$$

We rearrange and divide by $(\pi \Delta x {r_w}^2)$ to obtain Eq. (2.13)

$$\frac{\left(y_i \rho_i v_{i,x}\right)|_x - \left(y_i \rho_i v_{i,x}\right)|_{x+\Delta x}}{\Delta x} = \frac{-2\lambda \left(\rho_i v_{i,in}\right)|_{r=rw}}{r_w} \dots\dots\dots\dots\dots\dots\dots\dots\dots\dots (2.13)$$

As we indicated earlier, we assume the fluid properties are constant; therefore we cancel out the density. Also, we arrange Eq. (2.13) to obtain the differential form and take the limit of $\Delta x \to \infty$ as follows

$$\frac{d}{dx}\left(y_i v_{i,x}\right) = \frac{2\lambda v_{i,in}}{r_w} \dots\dots\dots\dots\dots\dots\dots\dots\dots\dots\dots\dots\dots\dots\dots\dots\dots\dots\dots\dots (2.14)$$

where "y_i" is the volume fraction of phase "i".

It is worth noting that we do not include the volumetric fraction in the inflow term since we assume single phase flow in the reservoir for each segment; Section Three explains the reservoir model in details.

Now, we use the finite difference approximation to obtain the discrete form of Eq. (2.14)

$$y_{i,j}v_{i,j} = y_{i,j-1}v_{i,j-1+}\frac{2\lambda v_{i,in}}{r_w} \ldots \ldots (2.15)$$

2.3 Momentum Balance

The aim of the momentum balance is to obtain equations to solve for the pressure drop in the pipe. As we did with the mass balance, we will first derive the equations for the single phase case then for the multiphase flow case.

2.3.1 Single Phase Flow

Eq. 2.16 represents the momentum balance mathematically;

$$\begin{pmatrix} Rate\ of \\ momentum\ in \end{pmatrix} = \begin{pmatrix} Rate\ of \\ Momentum\ out \end{pmatrix} - \begin{pmatrix} External\ force \\ on\ the\ fluid \end{pmatrix} \ldots \ldots (2.16)$$

We use the combined rate of momentum flux equation defined by Bird et al. (2002) which is shown by Eq. 2.17.

$$\Phi = \rho vv + p\delta + \tau \ldots \ldots (2.17)$$

The first term is the convective rate of momentum-flux tensor and the last two terms represent the molecular rate of momentum flux tensors. That is, all the terms have dimensions of momentum per unit time per unit area.

In our problem, we are only concerned about two components of the combined rate of momentum flux which can be expanded as follows

$$\Phi_{xx} = \rho v_x v_x + p + \tau_{xx} \quad (2.18)$$

and

$$\Phi_{rx} = \rho v_x v_r + \tau_{rx} \quad (2.19)$$

Furthermore, the component of the shear stress caused by flow along the x-direction and perpendicular to it can be expanded using Newton's law of viscosity and ignoring the dilatational viscosity as follows;

$$\tau_{xx} = -2\mu \frac{\partial v_x}{\partial x} + \frac{2}{3}\mu \frac{\partial v_x}{\partial x} = -\frac{4}{3}\mu \frac{\partial v_x}{\partial x} \quad (2.20)$$

For the third term in Eq. 2.16, we only consider force by gravity which represented by Eq. 2.21

$$\begin{pmatrix} External\ force \\ on\ the\ fluid \end{pmatrix} = -\pi R^2 \Delta x \rho g sin\theta \quad (2.21)$$

However, we will only consider horizontal or near horizontal wellbores so this gravity term will be neglected. Based on our geometry represented by Fig. 2.1, this term should take a negative sign since gravity is working against the flow if it is to the

surface, production well, and should take a positive sign for injection wells since gravity is working with the flow.

Eq. 2.19, 2.20 and 2.21 represent rate of momentum fluxes and have to be multiplied by the appropriate surface areas to obtain forces. Multiplying by the appropriate areas and substituting into Eq. 2.16 we obtain the following equation

$$\pi {r_w}^2 \left(\rho v_x v_x + p - \frac{4}{3}\mu \frac{\partial v_x}{\partial x}\right)|_{x=x} + 2\pi r_w \Delta x(\rho v_x v_r + \tau_{rx})|_{r=rw} = \left(\rho v_x v_x + p - \frac{4}{3}\mu \frac{\partial v_x}{\partial x}\right)|_{x=x+\Delta x} \quad (2.22)$$

We recall that (v_x) is assumed to be zero at the wall of the pipe so the term $\rho v_x v_r$ goes to zero. Also, we divide Eq. 2.22 by $(\pi {r_w}^2 \Delta x)$ to obtain

$$\frac{\left(\rho {v_x}^2 + p - \frac{4}{3}\mu \frac{\partial v_x}{\partial x}\right)|_{x=x}}{\Delta x} + \frac{2}{r_w}(\tau_{rx})|_{r=r_w} = \frac{\left(\rho {v_x}^2 + p - \frac{4}{3}\mu \frac{\partial v_x}{\partial x}\right)|_{x=x+\Delta x}}{\Delta x} \quad (2.23)$$

If we were to form the differential form of Eq. 2.23, the velocity derivative term would be a second derivative so for simplicity, we will neglect these terms and obtain Eq. 2.24

$$\frac{(\rho v_x^{\ 2} + p)|_{x=x}}{\Delta x} + \frac{2}{r_w}(\tau_{rx})|_{r=rw} = \frac{(\rho v_x^{\ 2} + p)|_{x=x+\Delta x}}{\Delta x} \quad (2.24)$$

Let us name the subscript "x" by "$j-1$" and the subscript "$x+\Delta x$" by "j" . Also, we will multiply Eq. 2.24 by Δx to obtain Eq. 2.25

$$(\rho v_x^{\ 2} + p)_{j-1} + \frac{2\Delta x}{r_w}(\tau_{rx})|_{r=rw} = (\rho v_x^{\ 2} + p)_j \quad (2.25)$$

We can solve Eq. 2.25 for the pressure at the current segment as shown by Eq. 2.26

$$p_j = p_{j-1} + \rho\left(v_{x,j-1}^{\ 2} - v_{x,j}^{\ 2}\right) + \frac{2\Delta x}{r_w}(\tau_{rx})|_{r=rw} \quad (2.26)$$

The shear stress on the wall (τ_{rx}) will be calculated using Fanning friction factor as shown by Eq. 2.27

$$\tau_{rx} = \frac{-\rho f v_x^{\ 2}}{2} \quad (2.27)$$

Substituting Eq. 2.27 into Eq. 2.26 we obtain

$$p_j = p_{j-1} + \rho\left(v_{x,j-1}^{\ 2} - v_{x,j}^{\ 2}\right) - \frac{\Delta x \rho f v_{x,j}^{\ 2}}{r_w} \quad (2.28)$$

Ouyang (1998) derived a modified correlation for the friction factor that accounts for the inflow effect. He noted that inflow into the wellbore increases friction factor

where outflow decreases the friction factor. His correlations are shown by Eq. 2.29 through Eq. 2.31.

$$f = \begin{cases} f_0(1 + \left(0.04304 {N_{Re,w}}^{0.6142}\right) \; laminar\ flow \ldots\ldots\ldots\ldots\ldots\ldots\ldots\ldots\ldots\ldots\ldots.\ldots. (2.29) \\ f_0(1 - \left(29.03 \left(\frac{N_{Re,w}}{N_{Re}}\right)^{0.8003}\right) \; Turbulent\ openhole\ completion \ldots\ldots\ldots. (2.30) \\ f_0(1 - \left(0.0153 {N_{Re,w}}^{0.3978}\right) \; Turbulent\ peforated \ldots\ldots\ldots\ldots\ldots\ldots\ldots\ldots\ldots (2.31) \end{cases}$$

where the Reynolds' numbers shown above are calculated by Eq. 2.24 and Eq. 2.25.

$$N_{Re,w} = \frac{2 r_w \rho v_{in}}{\mu} \ldots\ldots\ldots\ldots\ldots\ldots\ldots\ldots\ldots\ldots\ldots\ldots\ldots\ldots\ldots\ldots\ldots\ldots. (2.32)$$

$$N_{Re} = \frac{2 r_w \rho v_x}{\mu} \ldots\ldots\ldots\ldots\ldots\ldots\ldots\ldots\ldots\ldots\ldots\ldots\ldots\ldots\ldots\ldots\ldots\ldots. (2.33)$$

2.3.2 Multiphase Flow

Multiphase flow can occur when there is oil/water, oil/gas, water/gas or oil/water/gas flowing simultaneously in the pipe. We first derive the equations for the oil/water systems then for the gas/liquid systems.

In our model, we are going to treat oil/water systems using the homogeneous model in which mixture properties are calculated based on the volumetric ratio of oil and water in the flow. Also, we assume that the slip between the oil and water is negligible. Based on this assumption, the mixture velocity is

$$v_m = v_{so} + v_{sw}. \ldots\ldots\ldots\ldots\ldots\ldots\ldots\ldots\ldots\ldots\ldots\ldots\ldots\ldots\ldots\ldots\ldots\ldots. (2.34)$$

and the fraction of oil and water are calculated by Eq. 2.35 and 2.36

$$y_o = \frac{v_{so}}{v_{so} + v_{sw}} \quad \ldots\ldots (2.35)$$

$$y_w = 1 - y_o \quad \ldots\ldots (2.36)$$

and the mixture density is

$$\rho_m = y_o \rho_o + y_w \rho_w \quad \ldots\ldots (2.37)$$

For the mixture viscosity, Jayawardena (2000) developed a model for oil/water mixture viscosity that depends on determining which phase is dispersed and which is continuous. For our problem, the water will always be the dispersed phase and the oil will be the continuous phase since water cut considered in this study is not going to be high. Therefore the equation for the mixture viscosity is

$$\mu_m = \mu_o (1 - y_w)^{-2.5} \quad \ldots\ldots (2.38)$$

Also, Reynolds number will be calculated using Eq. 2.33 by replacing the single phase properties with the mixture properties. The inflow Reynolds number will be the same as Eq. 2.34 since we assume a single phase existing in each reservoir segment as will be shown in Section Three. Therefore, the pressure drop equation used will be

$$p_j = p_{j-1} + \rho\left(v_{m,x,j-1}{}^2 - v_{m,x,j}{}^2\right) - \frac{\Delta x \rho f v_{m,x,j}{}^2}{r_w} \quad \ldots\ldots (2.39)$$

If one of the flowing phases is gas, then we are going to use the model develop by Ouyang (1998) for gas/liquid flow which takes into account the effect of inflow on the frictional pressure drop. In this model, the liquid phase can consist of oil, water or both. If oil and water exist, they are going to be treated as a homogenous phase with

homogeneous properties calculated by Eq. 2.34 through Eq. 2.38. Ouyang's model requires knowing the in-situ gas void fraction. In order to do that, we implement the drift-flux model presented by Shi el al. (2005). First, we adopt the definition of the superficial velocities as follow

$$v_{sg} = \frac{q_g}{A_{pipe}} \quad \ldots\ldots (2.40)$$

and

$$v_{sl} = \frac{q_o + q_w}{A_{pipe}} \quad \ldots\ldots (2.41)$$

According to their model, the in-situ gas velocity is given by

$$v_g = v_{sg} + v_m + \frac{(1 - y_g)Ku}{y_g\sqrt{\frac{\rho_g}{\rho_l}} + 1 - y_g} * \left(\frac{\sigma_{gl} g(\rho_l - \rho_g)}{{\rho_l}^2}\right)^{\frac{1}{4}} \quad \ldots\ldots (2.42)$$

where y_g represents the in-situ gas void fraction given by the following equation

$$y_g = \frac{v_{sg}}{v_g} \quad \ldots\ldots (2.43)$$

And "Ku" is Kutateladze number (Schlumberger 2008) and is calculated using the following equations and the constant can be read from Table 2.1.

$$Ku = \begin{cases} 1.53 \; when \; y_g < 0.2 \\ Ku(D^*) \; as \; defined \; by \; table \; below \end{cases} \quad \ldots\ldots (2.44)$$

and the dimensionless diameter D^* is defined by Eq. (2.45)

$$D^* = \left[\frac{g(\rho_l - \rho_g)}{\sigma_{gl}}\right]^{0.5} D \ldots\ldots\ldots\ldots\ldots\ldots\ldots\ldots\ldots\ldots\ldots\ldots\ldots\ldots\ldots\ldots\ldots\ldots\ldots\ldots (2.45)$$

Table 2.1: Kutateladze Numbers as a Function of the Dimensionless Diameter, D*.

D*	Ku
≤2	0
4	1
10	2.1
14	2.5
20	2.8
28	3.0
≥50	3.2

The process of calculating y_g is iterative. First, the value of the in-situ gas velocity, v_g, is assumed to be equal to the superficial velocity, v_{sg}. Based on that, y_g is calculated using Eq. 2.43 and then this value is substituted in Eq. 2.42 to obtain a new value of the in-situ gas velocity, v_g. The values are compared and the calculation is continued until they converge given some desired tolerance.

Now, we can proceed with Ouyang's model. The model divides the pressure drop into four components caused by friction, gravity, acceleration due to inflow and acceleration due to fluid expansion. Mathematically, the model can be written as

$$p_j = p_{j-1} + \Delta x \left\{ \frac{dp}{dx}_f + \frac{dp}{dx}_g + \frac{dp}{dx}_{aW} + \frac{dp}{dx}_{aE} \right\} \ldots\ldots\ldots\ldots\ldots\ldots\ldots\ldots\ldots\ldots\ldots\ldots\ldots\ldots (2.46)$$

We also adopt the definitions of the following parameters from their model shown by Eq. 2.47 to 2.58; please refer to the nomenclature Section of the thesis for more on the definitions of these terms. The subscript "in" refers to inflow properties, "m" refers to mixture, "tp" refers to two-phase, "s" refers to superficial, "g" for gas and "*l*" for liquid.

$$q_{in,l} = nAv_{sl,in} \ldots\ldots\ldots\ldots\ldots\ldots\ldots\ldots\ldots\ldots\ldots\ldots\ldots\ldots\ldots\ldots\ldots\ldots\ldots\ldots\ldots\ldots\ldots\ldots\ldots\ldots (2.47)$$

$$q_{in,g} = nAv_{sg,in} \ldots\ldots\ldots\ldots\ldots\ldots\ldots\ldots\ldots\ldots\ldots\ldots\ldots\ldots\ldots\ldots\ldots\ldots\ldots\ldots\ldots\ldots\ldots\ldots\ldots\ldots (2.48)$$

$$q_{in,tp} = \frac{\rho_l}{\rho_{tp}} q_{in,l} + \frac{\rho_{lg}}{\rho_{tp}} q_{in,g} \ldots\ldots\ldots\ldots\ldots\ldots\ldots\ldots\ldots\ldots\ldots\ldots\ldots\ldots\ldots\ldots\ldots\ldots\ldots\ldots\ldots\ldots\ldots\ldots\ldots (2.49)$$

$$q_{in,m} = q_{in,l} + q_{in,g} \ldots\ldots\ldots\ldots\ldots\ldots\ldots\ldots\ldots\ldots\ldots\ldots\ldots\ldots\ldots\ldots\ldots\ldots\ldots\ldots\ldots\ldots\ldots\ldots\ldots\ldots (2.50)$$

$$v_{tp} = \frac{\rho_l}{\rho_{tp}} v_{sl} + \frac{\rho_{lg}}{\rho_{tp}} v_{sg} \ldots\ldots\ldots\ldots\ldots\ldots\ldots\ldots\ldots\ldots\ldots\ldots\ldots\ldots\ldots\ldots\ldots\ldots\ldots\ldots\ldots\ldots\ldots\ldots\ldots\ldots (2.51)$$

$$\beta_{aE} = \frac{\rho_{tp} v_m v_{sg}}{p} \ldots\ldots\ldots\ldots\ldots\ldots\ldots\ldots\ldots\ldots\ldots\ldots\ldots\ldots\ldots\ldots\ldots\ldots\ldots\ldots\ldots\ldots\ldots\ldots\ldots\ldots\ldots (2.52)$$

$$\rho_{tp} = \rho_l (1 - y_g) + \rho_g y_g \ldots\ldots\ldots\ldots\ldots\ldots\ldots\ldots\ldots\ldots\ldots\ldots\ldots\ldots\ldots\ldots\ldots\ldots\ldots\ldots\ldots\ldots\ldots\ldots\ldots\ldots (2.53)$$

$$\mu_{tp} = \mu_l (1 - y_g) + \mu_g y_g \ldots\ldots\ldots\ldots\ldots\ldots\ldots\ldots\ldots\ldots\ldots\ldots\ldots\ldots\ldots\ldots\ldots\ldots\ldots\ldots\ldots\ldots\ldots\ldots\ldots\ldots (2.54)$$

$$\rho_{in,m} = \rho_l \frac{q_{in,l}}{q_{in,m}} + \rho_g \frac{q_{in,g}}{q_{in,m}} \ldots\ldots\ldots\ldots\ldots\ldots\ldots\ldots\ldots\ldots\ldots\ldots\ldots\ldots\ldots\ldots\ldots\ldots\ldots\ldots\ldots\ldots\ldots\ldots\ldots\ldots (2.55)$$

$$\mu_{in,m} = \mu_l \frac{q_{in,l}}{q_{in,m}} + \mu_g \frac{q_{in,g}}{q_{in,m}} \ldots\ldots\ldots\ldots\ldots\ldots\ldots\ldots\ldots\ldots\ldots\ldots\ldots\ldots\ldots\ldots\ldots\ldots\ldots\ldots\ldots\ldots\ldots\ldots\ldots\ldots (2.56)$$

$$N_{Re,tp} = \frac{\rho_{tp} v_{tp} D}{\mu_{tp}} \quad \ldots\ldots (2.57)$$

$$N_{Re,wall} = \frac{\rho_{in,m} v_{in,m} D}{\mu_{in,m}} \quad \ldots\ldots (2.58)$$

Now, the frictional pressure component is

$$\frac{\partial p}{\partial x_f} = -\pi R \Delta x f_{tp} \rho_{tp} {v_{tp}}^2 \quad \ldots\ldots (2.59)$$

and the gravitational pressure drop is

$$\frac{\partial p}{\partial x_g} = -g \rho_{tp} sin\theta \quad \ldots\ldots (2.60)$$

and the accelerational pressure drop caused by fluid inflow is

$$\frac{\partial p}{\partial x_{aW}} = -\frac{1}{\pi R^2}\left(0.8\rho_{tp}\left(v_m q_{in,tp} + v_{tp} q_{in,m}\right) + 0.4\rho_{tp} v_m q_{in,tp}\right) \quad \ldots\ldots (2.61)$$

and finally the accelerational pressure drop caused by fluid expansion is

$$\frac{dp}{dx_{aE}} = \frac{\beta_{aE}}{(1-\beta_E)}\left\{\frac{dp}{dx_f} + \frac{dp}{dx_g} + \frac{dp}{dx_{aW}}\right\} \quad \ldots\ldots (2.62)$$

The friction factor is calculated using Eq. 2.29 through Eq. 2.31 but replacing the "$N_{Re,w}$" and "N_{Re}" by "$N_{Re,wall}$ "and "$N_{Re,tp}$ " defined by Eq. 2.58 and Eq. 2.57.

2.4 Energy Balance

The energy balance states that the rate of energy out is equal to the rate of energy in plus the rate of work done on the system. The convention is that if the work is done on

the system then it is positive and if it is done by the system then it is negative and the system loses energy.

2.4.1 Single Phase Flow

In the following derivation, we assume steady-state condition and we neglect the heat conduction in fluid and the effect of gravity since we consider horizontal or near horizontal wellbores. The energy balance can be written mathematically as follows

$$\pi R^2 e_x|_{x+\Delta x} = \pi R^2 e_x|_x + 2\pi R \Delta x e_r|_{r_w} \quad (2.63)$$

Using the definitions presented by Bird et al (2002), the rate of energy flux in the x-direction can be written as

$$e_x = \left(\frac{1}{2}\rho v^2 + \rho H\right) v_x + \tau_{xx} v_x + q_x \quad (2.64)$$

and for the rate of energy flux in the radial directions

$$e_r|_{r_w} = \left(\frac{1}{2}\rho {v_{in}}^2 + \rho H_{in}\right) v_{in} + \tau_{rr} v_{in} + q_{in} \quad (2.65)$$

We neglect the heat conduction in the fluid. Also, Yoshioka (2007) has noted from his model that the kinetic energy and viscous shear terms can be neglected without a loss in the accuracy of the solution. Therefore and for the sake of simplifying our derivation, we will ignore these terms; i.e. the "ρv^2" terms and "τv" terms. Therefore, Eq. 2.64 and Eq. 2.65 become

$$e_x = \rho H_x v_x + Q_x \quad (2.66)$$

$$e_r|_{r_w} = \rho H_{in} v_{in} + Q_{in} \text{ .... } (2.67)$$

where Q_x and Q_{in} are the rates of conductive heat fluxes and the subscripts indicate that the first is the rate of heat flux along the x-direction and latter is the rate of heat flux caused by the fluid inflow. The rate of conductive heat flux, Q_x, is through the fluid and as we indicated earlier we are going to assume that the conductive heat in the fluid is negligible and can be ignored. Therefore, Q_x wil be zero. On the other hand, Q_{in} is the rate of conductive heat flux between the formation and the fluid in the pipe caused by the difference between the temperature in the pipe fluid and the temperature in the formation adjacent to the wall of the pipe. Bird el al. (2002) showed a derivation for the expression for the rate of heat flux as a function of the difference between the fluid temperature and the wall temperate and the overall heat transfer coefficient as shown by Eq. 2.68

$$Q_{in} = U(T_{in} - T) = \frac{1}{r_w}\left\{\frac{ln\left(\frac{R_{cem}}{r_w}\right)}{K_{cem}} + \frac{ln\left(\frac{R_c}{r_w}\right)}{K_c} + \frac{1}{r_w h}\right\}^{-1} (T_{in} - T) \text{ .... } (2.68)$$

where U is the overall heat transfer coefficient, R_{cem} is the cement radius, R_c is the casing radius as shown by **Fig. 2.2**, K_{cem} is the cement conductivity, K_c is the casing conductivity, T_{in} is the temperature at the formation right adjacent to the wall of the pipe and T is the temperature of the fluid in the pipe. The parameter h is the heat transfer coefficient. For single phase flow, the correlation presented by Sieder and Tate (1936) will be used which is given by Eq. 2.69.

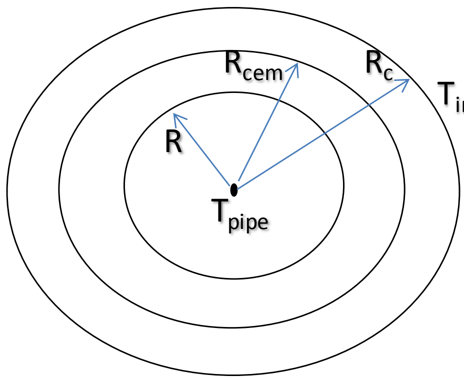

Fig. 2.2: A Cross-Sectional Area of a Pipe Showing the Various Pipe, Cement and Casing Radii and the Locations of Pipe Temperature and Inflow Temperature.

$$h = \frac{0.023 k {N_{Re}}^{0.8} Pr^{1/3}}{D} \quad \ldots\ldots\ldots\ldots\ldots\ldots\ldots\ldots\ldots\ldots\ldots\ldots\ldots\ldots\ldots\ldots\ldots\ldots\ldots\ldots\ldots\ldots\ldots\ldots.(2.69)$$

For gas/liquid systems, Kim and Ghajar (2002) presented two types of correlations for the heat transfer. In this work, we will use the correlation that is independent of the flow regime and is given by

$$\frac{h_{TP}}{(1-\alpha)h_L} = \left[1 + 0.27\left(\frac{x}{1-x}\right)^{-0.04}\left(\frac{\alpha}{1-\alpha}\right)^{-1.21}\left(\frac{Pr_G}{Pr_L}\right)^{0.66}\left(\frac{\mu_G}{\mu_L}\right)^{-0.72}\right] \ldots\ldots\ldots\ldots\ldots\ldots\ldots\ldots\ldots..(2.70)$$

where h_{TP} is the two-phase heat transfer coefficient and h_L is the single-phase heat transfer coefficient.

Substituting Eq. 2.68 into Eq. 2.67 and we obtain

$$e_r|_{r_w} = \rho H_{in} v_{in} + U(T_{in} - T) \ldots\ldots\ldots\ldots\ldots\ldots\ldots\ldots\ldots\ldots\ldots\ldots\ldots\ldots\ldots\ldots\ldots\ldots..\ldots(2.71)$$

Now, we substitute Eq. 2.71 and Eq. 2.66 into Eq. 2.63 and we get Eq. 2.72

$$\pi r_w{}^2 \rho H_x v_x|_{x+\Delta x} = \pi r_w{}^2 \rho H_x v_x|_x + 2\pi r_w \Delta x \gamma \rho H_{in} v_{in} + 2\pi r_w \Delta x (1 - \gamma) U(T_{in} - T)|_{r_w} \quad (2.72)$$

We note that in Eq. 2.72, we multiply the term $\rho H_{in} v_{in}$ by the segment open wall area, using the variable γ, and we multiply the term representing the heat conduction by the segment closed wall area, using the term (1-γ).

Now we rearrange Eq. 2.72, divide by "$\pi r_w{}^2 \Delta x$" and take the limit as Δx approaches zero to get the following differential form

$$\frac{\partial}{\partial x}(\rho H_x v_x) = \frac{2\gamma}{r_w} \rho H_{in} v_{in} + \frac{2\Delta x (1-\gamma)}{r_w} U(T_{in} - T) \quad (2.73)$$

To come up with a workable version of Eq. 2.73, we further expand the left hand side as follows using chain rule

$$\frac{\partial}{\partial x}(\rho H_x v_x) = \rho \frac{\partial}{\partial x}(H_x v_x) = \rho v_x \frac{\partial}{\partial x}(H_x) + \rho H_x \frac{\partial}{\partial x}(v_x) \quad (2.74)$$

Now we will expand the terms H_x and v_x more as follows. The enthalpy is defined as

$$H_x - H_x{}^0 = C_P(T - T^0) + \int_{p^0}^{p} \left[\hat{V} - T \left(\frac{\partial \hat{V}}{\partial T} \right)_{\tilde{p}} \right] d\tilde{p} \quad (2.75)$$

The specific volume,$\hat{V}$, is the inverse of density and the thermal expansion coefficient is defined by Eq. 2.76

$$\beta = -\frac{1}{\rho}\left(\frac{\partial \rho}{\partial T}\right)_p \ldots\ldots (2.76)$$

Therefore, we can write Eq. 2.75 as the following

$$H_x - {H_x}^0 = C_P(T - T^0) + \int_{p^0}^{p}\left[\frac{1}{\rho} - T\frac{\partial}{\partial T}\left(\frac{1}{\rho}\right)_{\tilde{p}}\right]d\tilde{p} \ldots\ldots (2.77)$$

We expand the term $T\frac{\partial}{\partial T}\left(\frac{1}{\rho}\right)$ using chain rule and incorporate the definition of thermal expansion and we end up with Eq. 2.78

$$H_x - {H_x}^0 = C_P(T - T^0) + \int_{p^0}^{p}\left[\frac{1}{\rho} - \frac{T\beta}{\rho}\right]d\tilde{p} \ldots\ldots (2.78)$$

The superscripts indicate the value of the property at standard conditions. The derivative of enthalpy then becomes

$$\frac{\partial}{\partial x}(H_x) = C_p\frac{\partial T}{\partial x} + \frac{1}{\rho}(1 - \beta T)\frac{\partial p}{\partial x} \ldots\ldots (2.79)$$

Moreover, Eq. 2.8 in a differential form becomes

$$\frac{\partial v_x}{\partial x} = \frac{2\lambda(v_{in}).}{r_w} \ldots\ldots (2.80)$$

Substituting (2.80) and (2.79) into (2.74) we obtain

$$\frac{\partial}{\partial x}(\rho H_x v_x) = \rho v_x C_p\frac{\partial T}{\partial x} + v_x(1 - \beta T)\frac{\partial p}{\partial x} + \rho H_x\frac{2\lambda(v_{in})}{r_w} \ldots\ldots (2.81)$$

Substituting equations (2.81) and (2.73) we get

$$\rho v_x C_p \frac{\partial T}{\partial x} + v_x(1-\beta T)\frac{\partial p}{\partial x} + \rho H_x \frac{2\lambda(v_{in})}{r_w} = \frac{2\gamma}{r_w}\rho H_{in} v_{in} + \frac{2\Delta x(1-\gamma)}{r_w} U(T_{in} - T) \quad (2.82)$$

Solving for the temperature derivative we get,

$$\frac{\partial T}{\partial x} = \frac{(\beta T - 1)}{\rho C_p}\frac{\partial p}{\partial x} + \frac{2\lambda v_{in}(H_{in} - H_x)}{v_x C_p r_w} + \frac{2(1-\gamma)}{\rho v_x C_p r_w} U(T_{in} - T) \quad (2.83)$$

Using equation (2.75) for the definition of enthalpy, and assuming that the pressure at the wall is the same as the pressure in the pipe, we end up with Eq. 2.84

$$H_{in} - H_x = C_P(T_{in} - T) \quad (2.84)$$

Substituting (2.84) into (2.83) we obtain

$$\frac{\partial T}{\partial x} = \frac{(\beta T - 1)}{\rho C_p}\frac{\partial p}{\partial x} + \frac{2\lambda v_{in}(T_{in} - T)}{v_x r_w} + \frac{2(1-\gamma)}{\rho v_x C_p r_w} U(T_{in} - T) \quad (2.85)$$

Rearranging and combining similar terms, the final form becomes

$$\frac{\partial T}{\partial x} = \frac{(\beta T - 1)}{\rho C_p}\frac{\partial p}{\partial x} + \frac{2}{\rho v_x C_p r_w}\big(\lambda \rho v_{in} C_p + (1-\lambda)U\big)(T_{in} - T) \quad (2.86)$$

We define a combined overall heat transfer coefficient that accounts for both the heat conduction through the pipe and heat convection by inflow fluid as shown by Eq. 2.87

$$U_{overall} = \lambda \rho v_{in} C_p + (1-\lambda)U \quad (2.87)$$

Joule-Thompson coefficient is defined by Eq. 2.88

$$K_{JT} = \frac{(\beta T - 1)}{\rho C_p}\frac{\partial p}{\partial x} \quad (2.88)$$

Substituting Eq. 2.87 and Eq. 2.88 into Eq. 2.86, we obtain

$$\frac{\partial T}{\partial x} = K_{JT}\frac{\partial p}{\partial x} + \frac{2}{\rho v_x C_p r_w} U_{overall}(T_{in} - T) \quad (2.89)$$

For our modeling purpose, we will use the finite difference to discretize the equation above. To simplify the manipulation process, we will introduce the following variables

$$A_1 = K_{JT} \quad (2.90)$$

$$A_2 = \frac{2}{\rho v_j C_p r_w} U_{overall} \quad (2.91)$$

Therefore, equation (2.89) becomes

$$T_j - T_{j-1} = \Delta x A_1 \frac{\partial p}{\partial x} + \Delta x A_2 \left(T_{in} - T_j\right) \quad (2.92)$$

Solving for "T_j" we obtain

$$T_j = \frac{T_{j-1} + A_1\left(p_j - p_{j-1}\right) + \Delta x A_2 T_{in}}{1 + \Delta x A_2} \quad (2.93)$$

Fig. 2.3 shows the variables used in Eq. (2.93). The equation states that difference in temperature between the current segment, segment "j", and the previous

segment, “j-1”, depends on three physical phenomena each represented by a term in Eq. (2.93).

The first terms shows that the temperature difference depends on the pressure drop and the coefficient that represents this relationship is Joule-Thompson coefficient. For liquids, Joule-Thompson coefficient is negative and the pressure drop is negative for a producing well. So, the result is a positive difference indicating a temperature rise. The second term in Eq. (2.93) relates the temperature change to the amount of heat from the incoming fluid. The heat inflow has two components; the conduction and the convection components. The combined effect is lumped in the overall heat transfer coefficient defined above. Moreover, the difference in temperature determines if it is heat added or taken out of the system. So, if the temperature at the wall, T_{in}, is higher than the pipe temperature, T_j, then heat will be added to the system which increases the temperature. The second term is divided by the specific heat capacity coefficient that determines that amount of temperature change based on the energy, heat, added or taken out of the system.

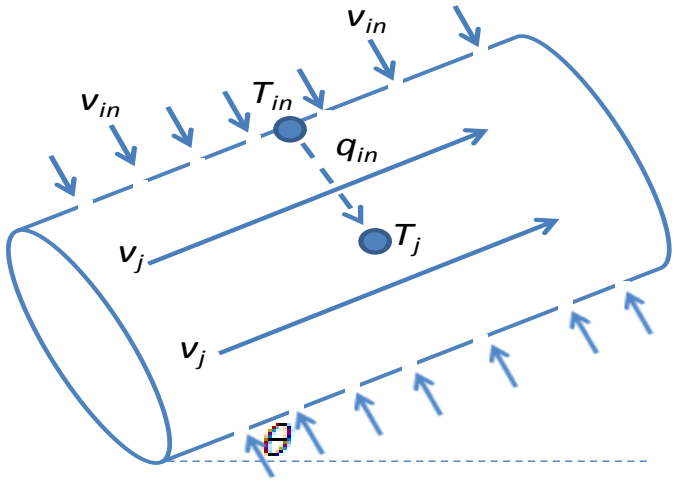

Fig. 2.3: Segment Diagram Showing the Variables in Eq. (2.93).

2.4.2 Multiphase Flow

For multiphase flow, we will write equation (2.89) for each phase as follows

$$(\rho v_x C_p y)_i \frac{\partial T}{\partial x} = (\rho v_x C_p y K_{JT})_i \frac{\partial p}{\partial x} + \frac{2}{R} U_{overall}(T_{in} - T) \quad \ldots\ldots\ldots\ldots\ldots\ldots\ldots\ldots\ldots\ldots (2.94)$$

where y_i is the in-situ fraction of the "*i*" phase calculated by the drift flux model presented above in the case of gas/liquid flow. Also, in reaching equation (2.95), we have assumed that the pressure and temperature in all phases will be the same. Applying equation (2.95) to all phases and summing them up with end up with equation (2.96)

$$\sum_i (\rho v_x C_p y)_i \frac{\partial T}{\partial x} = \sum_i (\rho v_x C_p y K_{JT})_i \frac{\partial p}{\partial x} + \frac{2}{R} U_{overall}(T_{in} - T) \quad \ldots\ldots\ldots\ldots\ldots\ldots\ldots\ldots (2.95)$$

Now, we solve for the temperature derivative

$$\frac{\partial T}{\partial x} = \frac{\sum_i \left(\rho v_x C_p y K_{JT}\right)_i}{\sum_i \left(\rho v_x C_p y\right)_i} \frac{\partial p}{\partial x} + \frac{2}{R \sum_i \left(\rho v_x C_p y\right)_i} U_{overall} (T_{in} - T) \quad (2.96)$$

We define the following variables

$$A_4 = \frac{\sum_i \left(\rho v_j C_p y K_{JT}\right)_i}{\sum_i \left(\rho v_j C_p y\right)_i} \quad (2.97)$$

$$A_5 = \frac{2}{R \sum_i \left(\rho v_j C_p y\right)_i} U_{overall} \quad (2.98)$$

The final discrete form is

$$T_j = \frac{T_{j-1} + A_4 \left(p_j - p_{j-1}\right) + \Delta x A_5 T_{in}}{1 + \Delta x A_5} \quad (2.99)$$

3. RESERVOIR MODEL

3.1 Introduction

As with the wellbore model, there are two equations we are interested in, the reservoir pressure and temperature models. These models have derived by Furui (2003), Dawkrajai (2006) and Yoshioka (2007) and in this Section we summarize their assumptions and results.

3.2 Reservoir Pressure Model

Furui (2003) derived a steady-state model for single phase flow for horizontal wells. **Fig. 3.1** and **Fig. 3.2** show the geometry of the model. The drainage area is box-shaped with the well centered spatially and fully penetrating the entire length of the reservoir. All fluid and rock properties are assumed constant and flow is assumed to be perpendicular to the well with no flow in the axial direction in the reservoir. Furui divided the reservoir based on the flow streamlines shape into linear and radial regions. By solving the diffusivity equation in each region and assuming continuity at the interface between the two, Furui was able to combine both solutions and his equation can be expressed as follows

$$q\ (BPD) = \frac{kL\left(P_e - P_{wf}\right)}{141.2\mu\left(ln\left(\frac{hI_{ani}}{r_w(I_{ani}+1)}\right) + \frac{\pi Y}{hI_{ani}} - 1.224 + s\right)} \ldots\ldots\ldots\ldots\ldots\ldots\ldots\ldots\ldots\ldots (3.1)$$

where q represents the production rate and k is the permeability.

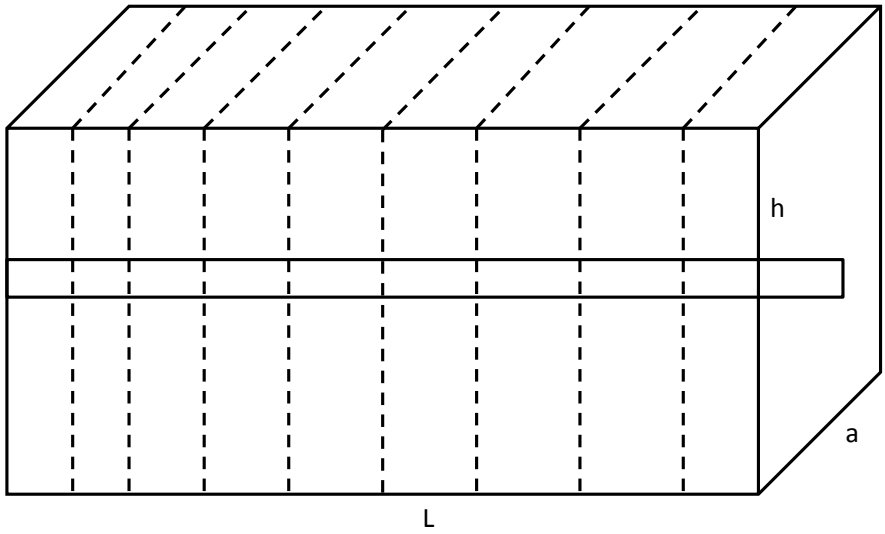

Fig 3.1: Reservoir Model Showing the Well at the Center.

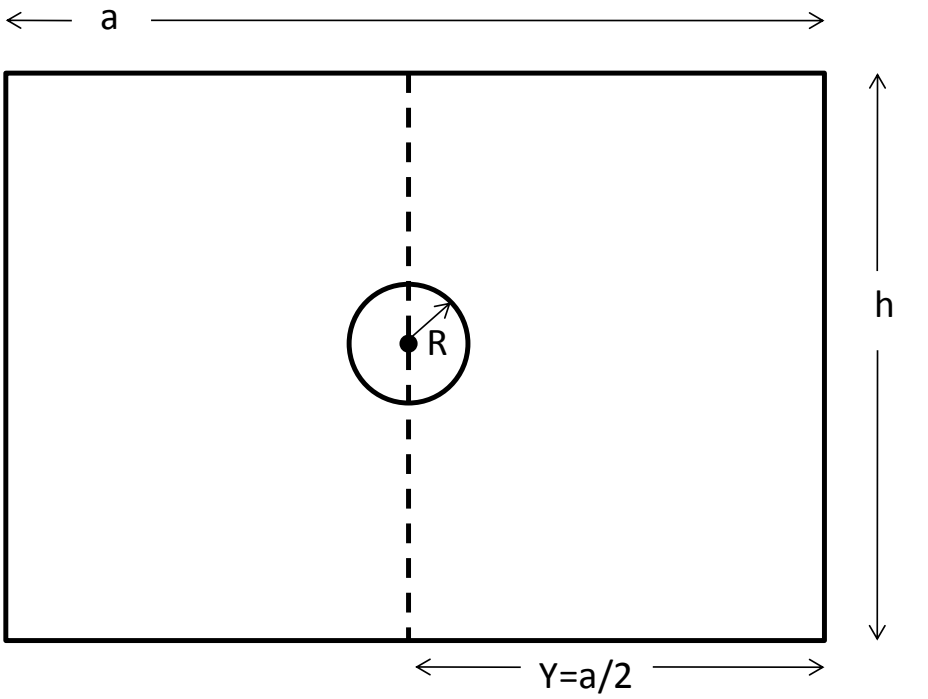

Fig 3.2: An End View Showing the Reservoir and Wellbore at the Middle.

The permeability variable in the Eq. 3.1 is calculated from the horizontal and vertical permeability by Eq. 3.2

$$k = \sqrt{k_H k_v} \quad \ldots\ldots (3.2)$$

Also, the anisotropy ratio,I_{ani}, is a factor introduced to account for the difference between the horizontal and vertical permeability and the impact that has on the production rate. The anisotropy ratio can be calculated as follows

$$I_{ani} = \sqrt{\frac{k_H}{k_v}} \quad \ldots\ldots (3.3)$$

3.3 Reservoir Temperature Model

The reservoir temperature has been derived first by Dawkrajai (2006) and then by Yoshioka (2007). In the model, the geometry was assumed to be exactly like the geometry assumed by Furui. The fluid and rock properties were assumed constant. The temperature model for the linear and radial regions were developed separately and combined using continuity conditions and two boundary conditions. One boundary condition defines the temperature at distance (y=Y), as shown by Fig. 3.2, and the other condition is the temperature of the wellbore. The differential equation of the reservoir temperature is

$$\rho C_p\left(\vec{u} \bullet \vec{\nabla} T\right) - \beta T\left(\vec{u} \bullet \vec{\nabla} p\right) - K_T \nabla^2 T + \vec{u} \bullet \vec{\nabla} = 0 \quad \ldots\ldots (3.4)$$

The temperature profile in the radial and linear regions are represented by Eq. 3.4 and Eq. 3.6 respectively

$$T(r) = \frac{1}{\beta} + c_0 r^{m0} + c_1 r^{m1} \qquad (3.6)$$

$$T(y) = \frac{1}{\beta} + c_2 e^{m2} + c_3 e^{m3} \qquad (3.7)$$

where "*y*" is the distance in the linear region of the reservoir and it goes from *y=h/2* to *y=a/2*, which is half the width.

The following is a list of the variables needed to evaluate the equations above

$$c_0 = \frac{\theta_3 + \theta_4}{\psi_1 + \psi_2} \qquad (3.8)$$

$$c_1 = \frac{\theta_1 + \theta_2}{\psi_1 + \psi_2} \qquad (3.9)$$

$$c_2 = \frac{l_3 + l_4}{\psi_1 + \psi_2} \qquad (3.10)$$

$$c_3 = \frac{l_1 + l_2}{\psi_1 + \psi_2} \qquad (3.11)$$

$$m_0 = \frac{q}{4\pi L}\left[\frac{\rho C_p}{K_T} + \sqrt{\left(\frac{\rho C_p}{K_T}\right)^2 + \frac{4\mu\beta}{kK_T}}\right] \qquad (3.12)$$

$$m_1 = \frac{q}{4\pi L}\left[\frac{\rho C_p}{K_T} - \sqrt{\left(\frac{\rho C_p}{K_T}\right)^2 + \frac{4\mu\beta}{kK_T}}\right] \qquad (3.13)$$

$$m_2 = \frac{q}{4hL}\left[\frac{\rho C_p}{K_T} + \sqrt{\left(\frac{\rho C_p}{K_T}\right)^2 + \frac{4\mu\beta}{kK_T}}\right] \qquad (3.14)$$

$$m_3 = \frac{q}{4hL}\left[\frac{\rho C_p}{K_T} - \sqrt{\left(\frac{\rho C_p}{K_T}\right)^2 + \frac{4\mu\beta}{kK_T}}\right] \ldots \ldots \ldots \ldots (3.15)$$

where K_T is the total conductivity of the rock and the fluid that saturates it. It is worth noting that only single phase is allowed to flow in the reservoir.

$$\theta_1 = e^{\frac{h}{2}(m_3+m_2)}\frac{h}{2}R^{m_0}(m_3 - m_2)(K_T m_0 - U_{overall}R)(\beta T_0 - 1) \ldots \ldots \ldots (3.16)$$

$$\theta_2 = \left(\frac{h}{2}\right)^{m_0}(\beta T_{well} - 1)U_{overall}R\left[e^{\frac{h}{2}m_3+\frac{Y}{2}m_2}\left(\frac{h}{2}m_3 - m_2\right) + e^{\frac{h}{2}m_2+\frac{Y}{2}m_3}\left(\frac{-h}{2}m_2 - m_3\right)\right] \ldots \ldots \ldots (3.17)$$

$$\theta_3 = e^{\frac{h}{2}(m_3+m_2)}\frac{h}{2}R^{m_1}(m_3 - m_2)(-K_T m_1 + U_{overall}R)(\beta T_0 - 1) \ldots \ldots \ldots (3.18)$$

$$\theta_4 = \left(\frac{h}{2}\right)^{m_1}(\beta T_{well} - 1)U_{overall}R\left[e^{\frac{h}{2}m_2+\frac{Y}{2}m_3}\left(\frac{h}{2}m_2 - m_1\right) + e^{\frac{h}{2}m_3+\frac{Y}{2}m_2}\left(\frac{-h}{2}m_3 - m_1\right)\right] \ldots \ldots \ldots (3.19)$$

$$\psi_1 = \beta R^{m_1}\left(\frac{h}{2}\right)^{m_1}(K_T m_1 - U_{overall}R)$$

$$\left[e^{\frac{h}{2}m_2+\frac{Y}{2}m_3}\left(\frac{h}{2}m_2 - m_0\right) + e^{\frac{h}{2}m_3+\frac{Y}{2}m_2}\left(\frac{-h}{2}m_3 + m_0\right)\right] \ldots \ldots \ldots (3.20)$$

$$\psi_2 = \beta R^{m_0}\left(\frac{h}{2}\right)^{m_1}(K_T m_0 - U_{overall}R)$$

$$\left[e^{\frac{h}{2}m_3+\frac{Y}{2}m_2}\left(\frac{h}{2}m_3 - m_1\right) + e^{\frac{h}{2}m_2+\frac{Y}{2}m_3}\left(\frac{-h}{2}m_2 + m_1\right)\right] \ldots \ldots \ldots (3.21)$$

$$l_1 = R^{m_0}e^{\frac{h}{2}m_2}(-K_T m_o + U_{overall}R)(\beta T_0 - 1)\left(\frac{h}{2}\right)^{m_1}\left(\frac{h}{2}m_2 - m_1\right) \ldots \ldots \ldots (3.22)$$

$$l_2 = \left(\frac{h}{2}\right)^{m_o}\left[e^{\frac{h}{2}m_2}R^{m_1}\left(\frac{-h}{2}m_2 + m_1\right)(-K_T m_1 + U_{overall}R)(\beta T_0 - 1)\right.$$
$$\left. + e^{\frac{Y}{2}m_2}U_{overall}R\left(\frac{h}{2}\right)^{m_1}(\beta T_{well} - 1)(m_1 - m_0)\right] \ldots\ldots\ldots\ldots\ldots\ldots (3.23)$$

$$l_3 = R^{m_1}e^{\frac{h}{2}m_2}(K_T m_o + U_{overall}R)(\beta T_0 - 1)\left(\frac{h}{2}\right)^{m_1}\left(\frac{h}{2}m_2 + m_1\right) \ldots\ldots\ldots\ldots\ldots (3.24)$$

$$l_4 = \left(\frac{h}{2}\right)^{m_o}\left[e^{\frac{h}{2}m_2}R^{m_1}\left(\frac{h}{2}m_2 - m_0\right)(-K_T m_1 + U_{overall}R)(\beta T_o - 1)\right.$$
$$\left. - e^{\frac{Y}{2}m_3}U_{overall}R\left(\frac{h}{2}\right)^{m_1}(\beta T_{well} - 1)(m_1 - m_0)\right] \ldots\ldots\ldots\ldots\ldots\ldots (3.25)$$

4. COUPLED WELLBORE AND RESERVOIR MODEL

4.1 Introduction

The objective of this research is to develop a model that couples the flow from two or three horizontal laterals into one motherbore as shown by **Fig. 4.1**. The program will calculate the pressure and temperature profiles along the motherbore in multilateral wells. In the following Sections, we describe the development of this model.

4.1.1 Multilateral Well Model Assumptions

First of all, we start by explaining the geometry and terminology that will be used for the model. Fig. 4.1 is top view diagram of a trilateral well. As we can see, the three horizontal wellbores, or laterals, are connected to one main conduit or a motherbore at the subsurface level. The individual horizontal laterals are shown by the dotted green rectangles and lines and their respective drainage areas are shown by dotted orange rectangles. As we explained in Section Three, the drainage areas will be boxed-shaped in three-dimensional frame work. It is worth mentioning that these orange rectangles are not connected which signifies the assumption that the laterals drain separate and non-communicating reservoirs.

As shown by the legends in Fig. 4.1, the blue boxes represent the packers which prevent the fluid to flow in the annulus between the tubing and the casing forcing the flow to go into the tubing. The red circles represent the inflow choke valves which can be adjusted to restrict the flow from a certain lateral or to eliminate the production from that lateral completely. The arrows show the direction of flow in the system.

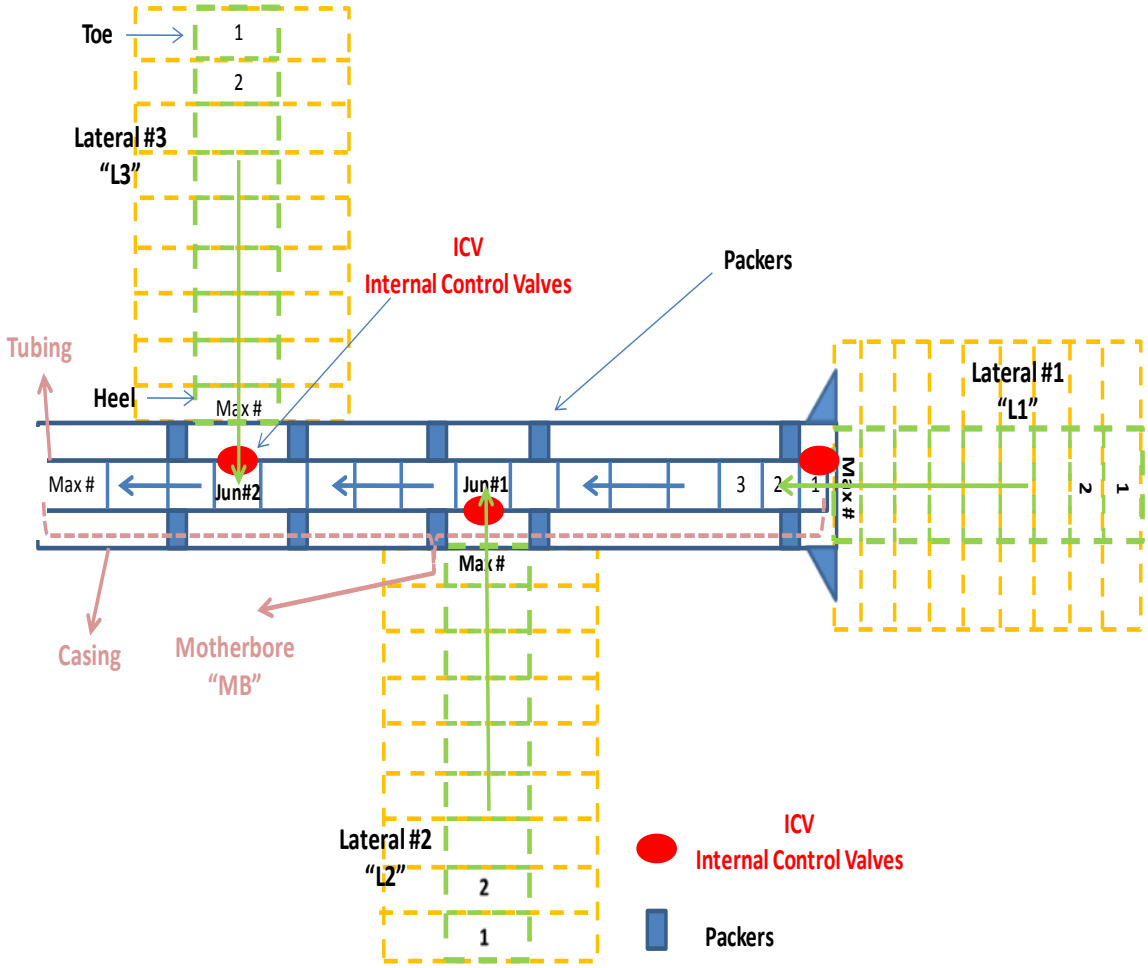

Fig. 4.1: A Diagram of Three Laterals Connected to a Motherbore that Shows the Segmentations, the Location of The Valves and Packers.

Throughout this thesis, regarding a horizontal lateral, a toe segment is the one furthest away from the motherbore and a heel segment is the one adjacent and connected to the motherbore as shown by lateral #3 in Fig 4.1.

In our model, each lateral is treated like a separate horizontal well. That is, the reservoir is segmented as shown by Fig. 3.1 and Fig. 4.1 so that only one phase is allowed to flow in each segment. However, different segments can have different phases flowing. One reservoir segment can flow oil and the other segment can flow water and multiphase flow can occur in the wellbore.

Moreover, the reservoir model assumes that the drainage area for each lateral is defined and in our model we will assume that the information is provided as an input. It is also assumed that the laterals do not interfere with each other in the reservoir. This assumption holds correct if laterals are drilled in different, non-communicating formations. The assumption is reasonable when laterals are drilled far apart from each other so that inference effect can be neglected. When all the laterals are allowed to produce, their production is commingled in the motherbore and that is how a lateral's performance can affect other laterals' production. For example, laterals drilled in high pressure reservoirs will tend to choke the production for other laterals and dominate the flow.

The rock properties are assumed to be provided by the user and are assumed to be constant throughout the calculation. Also, the fluid properties can either be provided by the user or calculated from common correlations in the petroleum literature presented by McCain (1990) and Prats (1982). The properties will be given, or calculated, at average pressure and temperature values that are expected for a specific run and will then be assumed constant throughout the calculation.

As we have indicated, the aim of the study is to calculate the pressure and temperature profile along the motherbore. The laterals and the motherbore are assumed to be horizontal or near horizontal with only slight inclination. Therefore, there will be a slight temperature variation which should not alter the properties significantly. Moreover, the reservoir pressure in all the cases that we consider is above 2,500 psi and the pressure change in the reservoir will be mostly between 100 -200 psi with the exception of two runs where the drawdown pressure was 300 psi. Under these conditions, the change in the oil and water properties will not be significant and is assumed to have negligible effect on the results.

4.2 Coupled Pressure Model

The solution process starts with solving for the pressure in each lateral and in the motherbore. The process is illustrated by **Fig. 4.2** and starts by assuming a pressure profile in the first lateral, L1. Based on Eq. 3.1, the inflow rates are calculated. After that, if multiphase flow exists, then we calculate the fraction of each phase using Eq. 2.35 through Eq. 2.37 for oil/water system. If we deal with gas/liquid flow, then Eq. 2.40 through Eq. 2.45 are used to estimate the in-situ gas and liquid fractions.

After that, we calculate the pressure drop in the lateral. To do so, we use Eq. 2.28 for single phase, Eq. 2.39 for oil/water two-phase flow or Ouyang's model for gas/liquid flow represented by Eq. 2.46 through Eq. 2.62. Once the pressure drop is calculated, a new pressure profile will be obtained. The new pressure profile is compared to initial assumed profile, if both profiles converge, given a desired tolerance, then the process is terminated. Otherwise, the new pressure profile is used to calculate the inflow

rates and process is repeated until convergence is achieved. This procedure is illustrated by Fig. 4.2. Eq. 4.1 shows the convergence criteria used in our calculation.

$$\frac{(\boldsymbol{p}^j - \boldsymbol{p}^{j+1})^T(\boldsymbol{p}^j - \boldsymbol{p}^{j+1})}{(\boldsymbol{p}^j)^T(\boldsymbol{p}^j)} < 10^{-6} \quad \ldots \ldots \ldots \ldots \ldots \ldots \ldots \ldots \ldots \ldots \ldots \ldots \ldots \ldots \ldots \ldots \ldots \ldots \ldots \ldots \ldots \ldots \ldots \ldots \ldots \ldots \ldots \ldots \ldots \ldots \ldots \ldots \ldots \ldots \ldots \ldots \ldots \ldots \ldots \ldots \ldots \ldots \ldots \ldots \ldots (4.1)$$

where "$\boldsymbol{p}$" is the pressure vector representing the wellbore pressure and the superscripts indicate the different iterations.

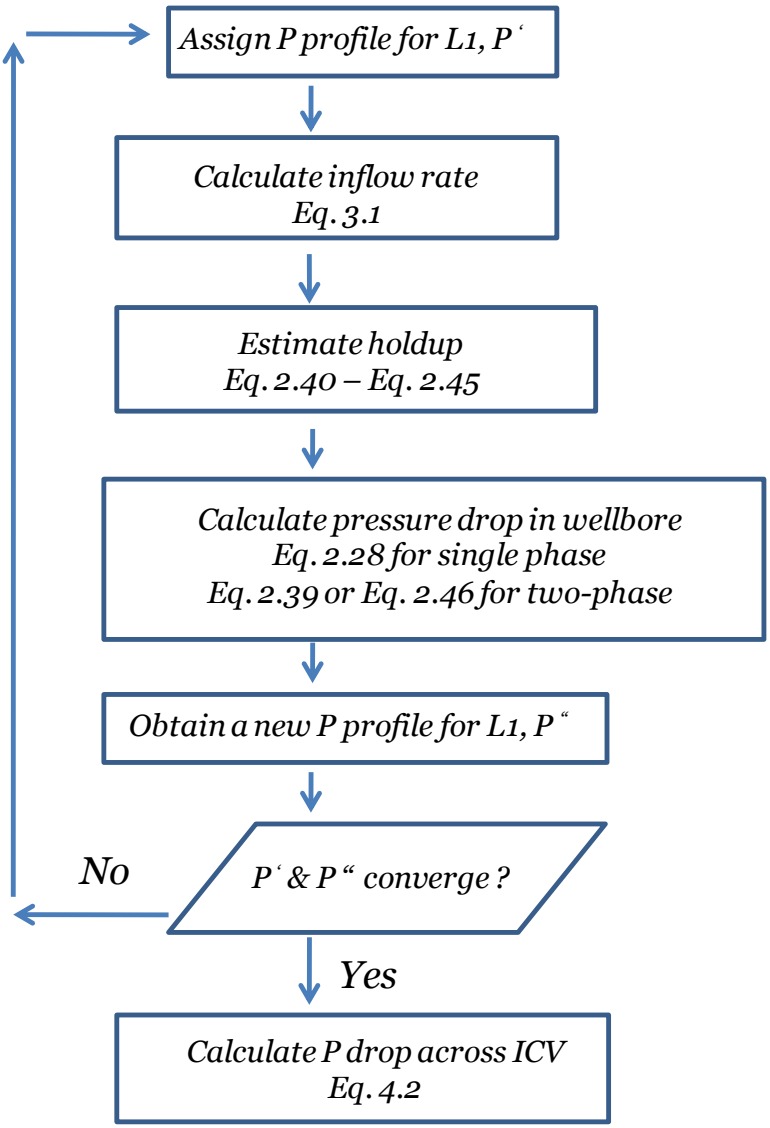

Fig. 4.2: Pressure Calculation Process in Each Lateral.

The total flow from L1 enters the wellbore at the toe of the motherbore, shown as segment #1 in Fig. 4.1. The flow rate is the total flow rate for each phase from all segments but we still have to calculate the pressure at the toe of the motherbore. As the flow enters the motherbore, it passes through the ICV, or the inflow control valve, where it is subjected to a pressure drop. These valves open in an incremental fashion going from position one to ten with each position having a different open area. To estimate the pressure drop, we use a correlation for a specific type of ICV as shown by Eq. 4.2

$$\Delta p = \left(\frac{q}{CV}\right)^2 \hat{\rho} \quad \ldots\ldots (4.2)$$

where $\hat{\rho}$ is the specific density of the fluid and values of the "CV" coefficient depends on the size of the opening of the valve as shown by Table 4.1. In Eq. 4.2, "q" represents the flow rate with dimension "volume/time", the "CV" factor has dimension of "volume/time/square root of pressure" and the specific density is dimensionless.

Notice that "CV" values are equipment dependent and the values in Table 4.1 only apply to one type of ICV. The values are used here to illustrate the procedure of calculation.

Table 4.1: The Values of the CV Coefficient for a Smart Completion Valve, Valve size is 3-1/2".

Valve Position	CV gpm/psi$^{1/2}$
1	1.1
2	2.4
3	4.4
4	6.8
5	9.4
6	14.3
7	25.4
8	42.4
9	105
10	175

"*gpm"* in Table 4.1 stands for gallon per minute. Once the pressure drop across the valve is determined, the pressure at segment #1 of the motherbore is set to be equal to the pressure at the heel of L1 less the pressure drop across the ICV as shown by Eq. 4.3

$$p_{MB,1} = p_{lateral\#1,N} - \Delta p_{valve} \quad (4.3)$$

Subscript "*N*" indicates that heel segment of lateral #1.

Once the pressure at the toe of the motherbore is calculated by Eq. 4.3, we advance to the next segment in the motherbore. **Fig. 4.3** summarizes the pressure calculation procedure in the motherbore. If the next segment is not a junction segment,

then we calculate the pressure drop between the segments using Eq. 2.28 for single phase, Eq. 2.39 for oil/water two-phase flow or Eq. 2.46 through Eq. 2.62 for gas/liquid flow. The process continued up to the segment where the next lateral is located, or Jun#1 as shown on Fig. 4.1. The value of the pressure at that junction segment is calculated and let us call it $p_{jun\#1}$. After that, the process of calculating the inflow rates and pressure profile in L2 is started in a similar manner as was the case with L1. Then, the pressure drop across the second valve is calculated using Eq. 4.2 and we calculate a pressure at Jun#1 using Eq. 4.3 and let us call it $p^{L2}{}_{jun\#1}$. Now, we compare $p^{L2}{}_{jun\#}1$ to $p_{jun\#1}$, if the value do not converge within a given tolerance, a different pressure profile is assumed in L2 and the inflow and pressure calculations are repeated until $p^{L2}{}_{jun\#}1$ converges to $p_{jun\#1}$. This process ensures pressure equilibrium in the system.

After the calculations at Jun#1 are done, we advance in the motherbore and calculate the pressure profile until we reach the next junction point for Lateral #3, L3, or Jun#2. We repeat the same process as we did with Jun#1. Then, we proceed again in the motherbore with the pressure profile calculation until we reach the heel of the motherbore.

As part of the input, the flowing bottomhole pressure at the heel of the motherbore is specified and let us call it $p_{MB,heel}$. Our program will calculate pressure at the heel of the motherbore and let us call it $p^{Calc}{}_{MB,heel}$. The value $p^{Calc}{}_{MB,heel}$ is compared to the specified value $p_{MB,heel}$, if it converges within a certain tolerance, the pressure calculation is terminated; otherwise the process will be restarted with L1 and by

assuming a different pressure profile. The reason for this last step is that the value $p_{MB,heel}$ is the one that operators can normally control and monitor.

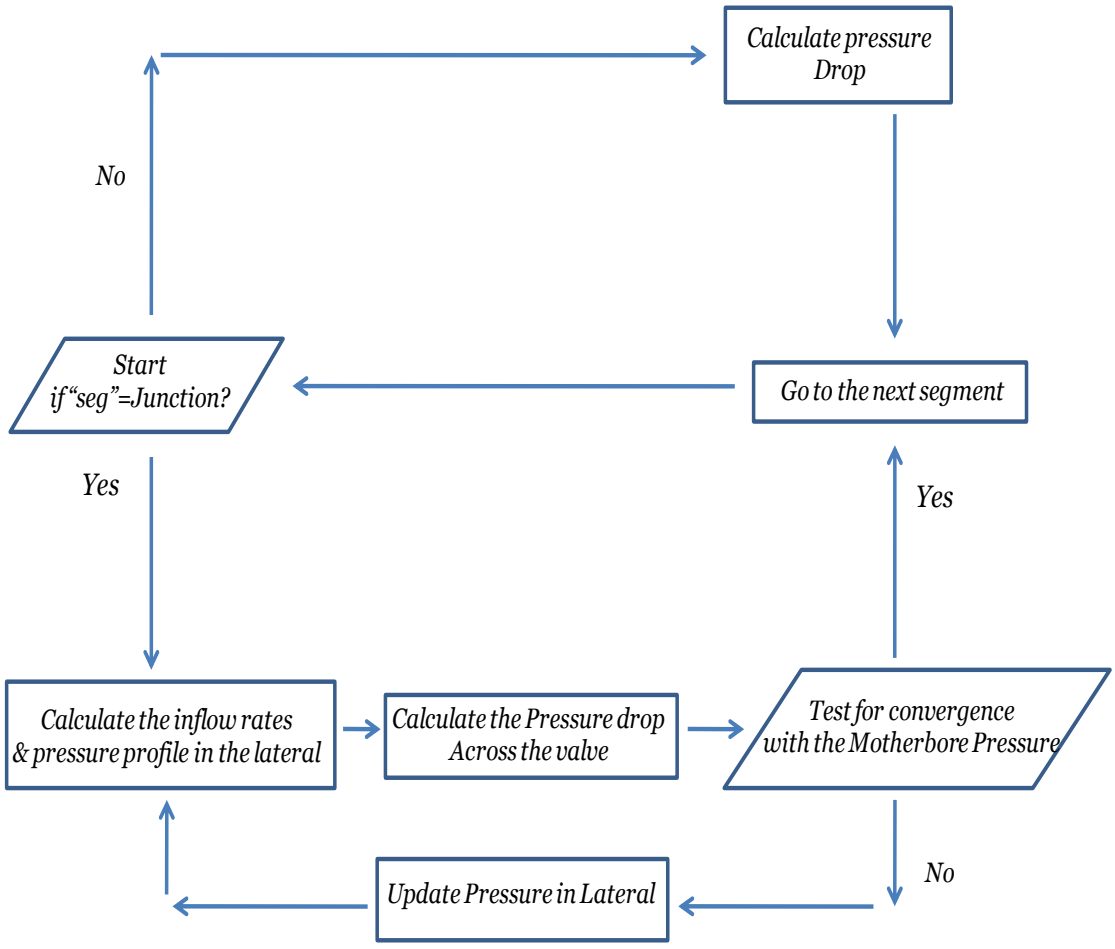

Fig. 4.3: Pressure Calculation Process in the Motherbore.

4.3 Coupled Temperature Model

4.3.1: Temperature Calculation in Each Lateral

Once the pressure profiles are calculated in the motherbore and in each lateral, we then proceed with calculating the temperature profile in the system. We first start with L1 and from the toe segment, segment #1. In Sections 2 and 3, we derived the wellbore and temperature models represented by Eq. 2.94 for single phase and Eq. 2.101 for multiphase. We also showed the equation for the reservoir temperature model represented by Eq. 3.6. These equations are shown below for reference.

$$T_j = \frac{T_{j-1} + A_1(p_j - p_{j-1}) + \Delta x A_2 T_{in}}{1 + \Delta x A_2} \qquad (2.93)$$

$$T_j = \frac{T_{j-1} + A_4(p_j - p_{j-1}) + \Delta x A_5 T_{in}}{1 + \Delta x A_5} \qquad (2.99)$$

$$T(r) = \frac{1}{\beta} + c_0 r^{m0} + c_1 r^{m1} \qquad (3.6)$$

In our model, we need to calculate the temperature at the wall of the lateral which is T_{in} in our notation. Therefore, Eq. (3.6) is evaluated at a distance equivalent to the wellbore radius, r_w. Also, we note that the wellbore temperature, T_j, is a function of the fluid properties in the pipe, wellbore geometry and the reservoir inflow temperature, T_{in} as shown by Eq. 2.94 and Eq. 2.101. Also, the reservoir inflow temperature, T_{in}, is a function of the reservoir fluid properties, the inflow rate, reservoir geometry and the wellbore temperature at each segment, i.e. T_j, as shown by Eq. 3.6. Eq. 3.6 does not show the dependency on the wellbore temperature however the calculation of the

coefficients, C_0 and C_1, require the wellbore temperature, T_j, to be known. So, we can see that for each segment we have two equations with two unknowns which should be solved iteratively. This process is explained by the flow chart given by **Fig. 4.4**.

However for the first segment, toe segment, of each lateral, we make the assumption that there is no heat flux at wellbore. Therefore for the first segment of each lateral, our boundary conditions will be the reservoir temperature at the outer boundary and no heat flux at the inner boundary. This enables us to calculate the reservoir inflow temperature, T_{in}. Then the wellbore temperature, T_j, is assumed to be equal to the reservoir inflow temperature. However for the subsequent segments, we assume a temperature profile in the wellbore which then enables us to obtain estimates for the inflow temperatures at each segment, T_{in} or T(rw), using Eq. 3.6. After that, we apply Eq. 2.94 or Eq. 2.101 to recalculate the wellbore temperatures. The recently calculated values are compared with the temperature profile assumed; if the values converge within a certain tolerance, the process is terminated. Otherwise, the temperature profile is updated and the process it repeated until convergence is obtained.

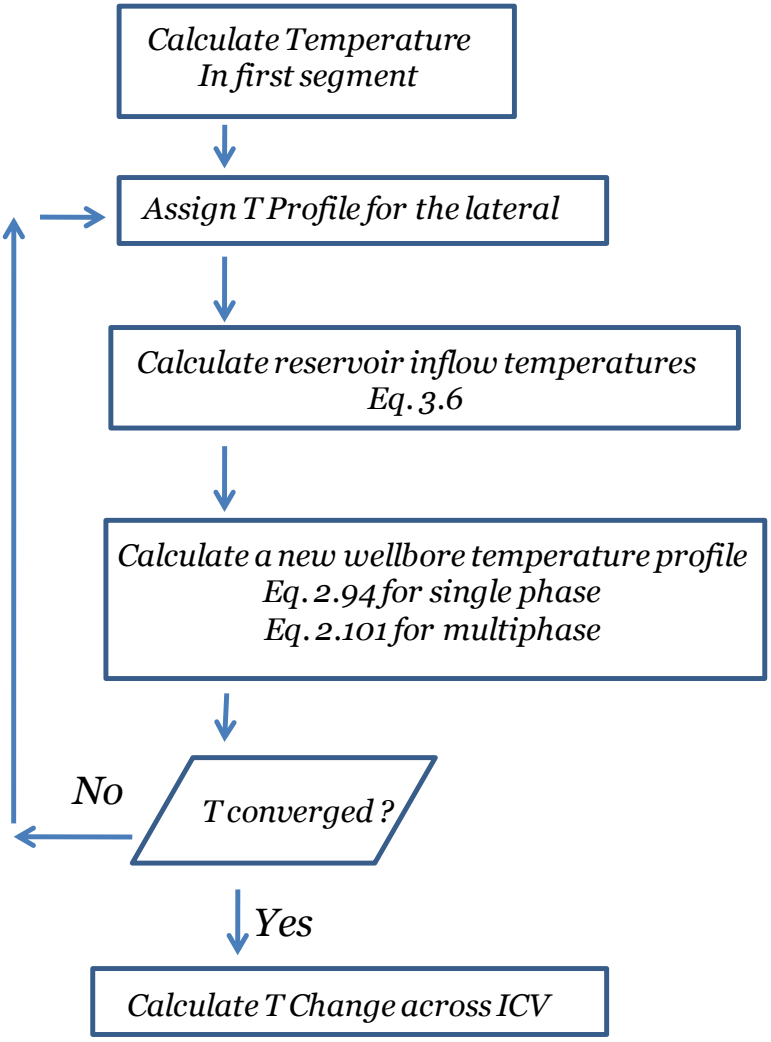

Fig. 4.4: Wellbore Temperature Calculation Procedure in Each Lateral.

As we have shown in the pressure model calculation, there will be a pressure drop across the smart completion valve and an associated temperature rise or drop depending on the fluid type. To calculate this temperature change across the valve, we use Eq. 4.3 for single phase flow or we use Eq. 4.4 to calculate the associated temperature change for multiphase flow. In these equations, we use Joule-Thompson coefficient to convert the pressure drop into a temperature change.

For single phase;

$$\Delta T = K_{JT}\Delta P_{across\ valve} \quad \ldots\ldots (4.3)$$

For multiphase phase;

$$\Delta T = \frac{\sum_i \left(\rho v_x C_p y K_{JT}\right)_i}{\sum_i \left(\rho v_x C_p y\right)_i}\Delta P_{across\ valve} \quad \ldots\ldots (4.4)$$

4.3.2: Temperature Calculation in the Motherbore

The temperature profile in the motherbore is calculated after the temperature profile in each lateral is determined. The calculation is started from the toe of the motherbore, lowest segment. As shown by **Fig. 4.5**, the flow rate, pressure and temperature have been determined at the heel of lateral #1, L1. To calculate the temperature at the first segment in the motherbore, we add the temperature change across the valve to the temperature at the heel of lateral #1, or L1. This temperature change is caused by the pressure drop and is calculated using Eq. 4.3 or Eq. 4.4.

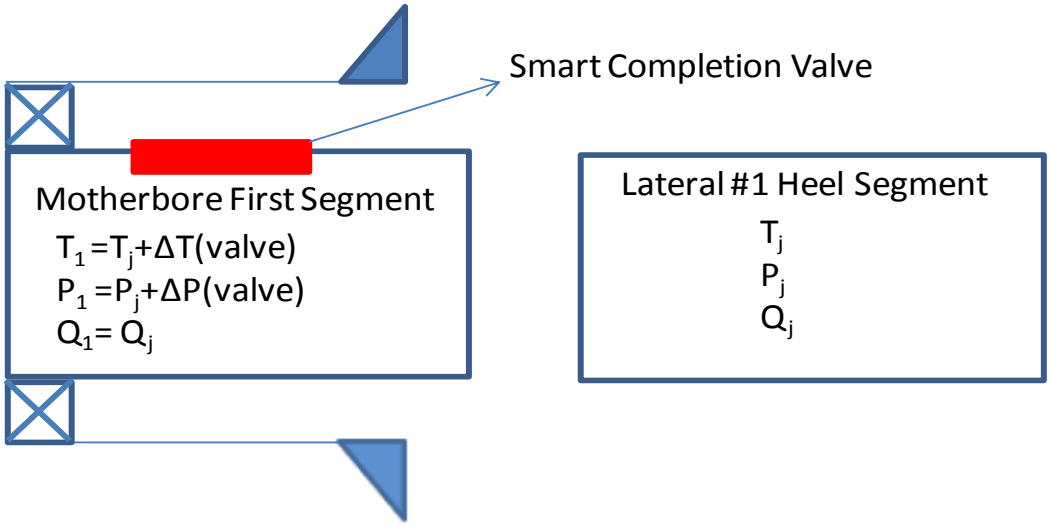

Fig. 4.5: Diagram Showing the Calculation Variables for the First Segment in the Motherbore.

For the subsequent segments in the motherbore, Eq. 2.94 or Eq. 2.101 is used for single phase flow or multiphase flow respectively and the inflow terms are dropped since there is no inflow. For example, Eq. (2.94) becomes

$$T_j - T_{j-1} = \Delta x K_{JT} \frac{\partial p}{\partial x} \quad (4.5)$$

Eq. (4.5) shows that the temperature rise between any two segments will be mainly caused by the pressure drop between the segments.

For the segments that are junction points; that is, segments where laterals intersect the motherbore, we apply Eq. 2.94 or Eq. 2.101 however with some modifications to the variables used. As shown by **Fig. 4.6**, variables with subscript "L" indicate that the value is calculated for the lateral and variables with subscript "M" indicate that the value is calculated for the motherbore. Subscripts "j" and "j-1" indicate a segment and its predecessor. Eq. 4.6 shows the form of the equation used.

$$T_{M,j} - T_{M,j-1} = K_{JT}\left(p_{M,j} - p_{M,j-1}\right) + \frac{2\lambda\Delta x}{v_{M,j}R} v_L\left(T_L - T_{M,j}\right)$$
$$+ \frac{2\Delta x}{\rho v_{M,j} C_p R}(1-\lambda)U\left(T_L - T_j\right) \ldots \ldots \ldots \ldots (4.6)$$

On the right hand side, Eq. 4.6 has four terms; the first term shows the contribution to the temperature difference caused by the pressure drop. The second term represents the convective component of the heat transfer caused by the inflow of fluid from the lateral which is at a different temperature, T_L. Note that the term is multiplied by the percentage of the total area open for flow, λ. So if the valve is closed, there will be no convective heat transfer. The third term represented the conductive component of the heat transfer. It takes the difference between the temperature coming for the lateral and the segment temperature and then this difference is multiplied by the heat transfer coefficient, U, to determine the heat flux rate. This rate is divided by "ρvCp" term which represents the amount of heat flux rate required to raise the temperature by on degree. Whether the temperature rises or drops depends on whether heat is put into the system or taken out of the system which is determined by the difference between the temperature of the fluid coming from the lateral, T_L, and the segment temperature, $T_{M,j}$. That is, the segment will lose energy if "T_L" is lower than "$T_{M,j}$" and vice versa. Note that the third term is multiplied by (1-λ) which represents the closed area of the pipe.

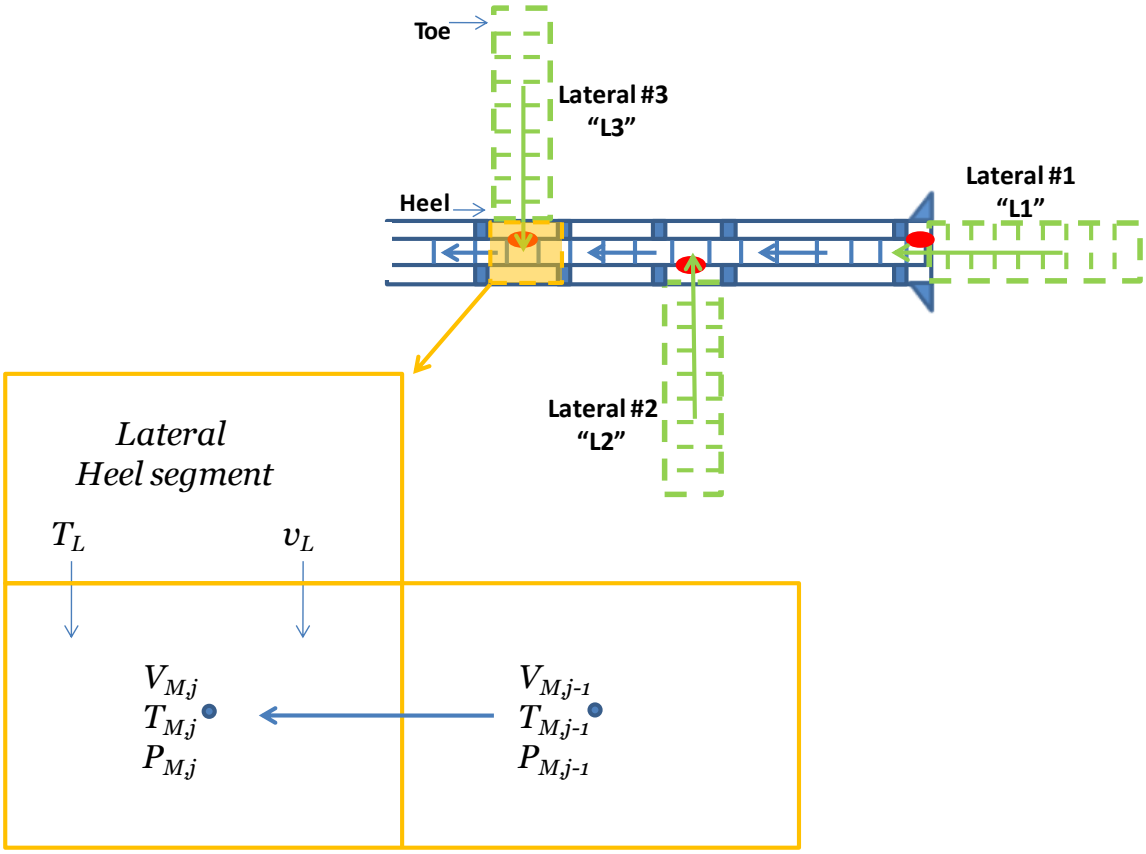

Fig. 4.6: Diagram Showing the Variables in a Junction Segment.

5. RESULTS AND DISCUSSION

5.1 Results for Horizontal Wells

In this Section, we will show some important results for the pressure and temperature profiles for horizontal wells. Although our work focuses on multilateral wells, results from horizontal well cases will help us interpret and understand multilateral well results. Data used for the horizontal well is shown on Table 5.1 and Table 5.2.

Table 5.1: Reservoir and Wellbore Data Summary for the Horizontal Well Case.

a (ft)	3000	D (in)	6	Skin	0
h (ft)	50	Roughness	0.01	T_0 (F)	180
L (ft)	2000	Pe (psi)	2800	K_T (Btu/hr-ft-F)	2
k (mD)	63	Pwf (psi)	2700	# of Segments	100
Angle (degrees)	0				

Table 5.2: Fluid Properties Used for Oil.

Viscosity (cP)	0.76
Density (Ib_m/ft^3)	43.0
Specific Heat Capacity (Btu/Ib_m-F)	0.504
Thermal Expansion Coefficient (1/F)	0.000465
K_{Tt} (Btu/hr-ft-F)	2

Fig. 5.1 shows a plot of the pressure profile along the horizontal well and **Fig. 5.2** shows the resulting temperature profile; other important results are summarized in Table 5.3.

Table 5.3: Main Results from Horizontal Well Simulation.

Oil Rate (BPD)	8,565
Temperature Differential Across Horizontal lateral (F)	0.02
Pressure Differential Across Horizontal Lateral (psi)	-1.93
The Inflow Temperature, T_{in} (F) @ Toe of Horizontal Lateral	184.02

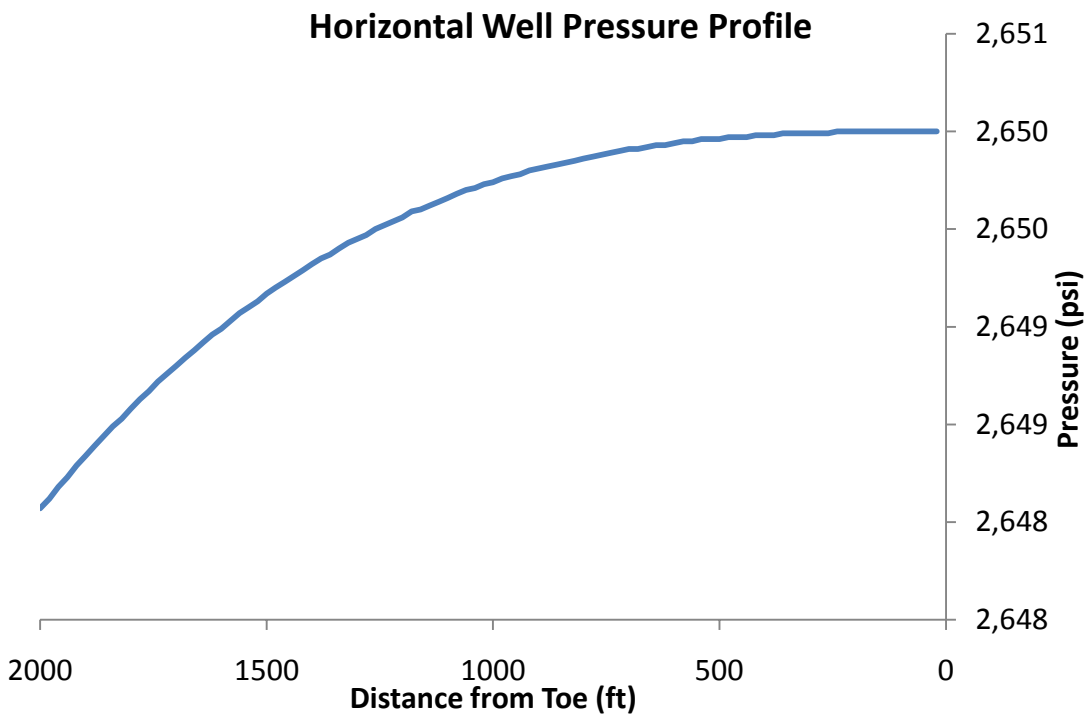

Fig. 5.1: Pressure Profile for a Horizontal Well; 6” in Diameter.

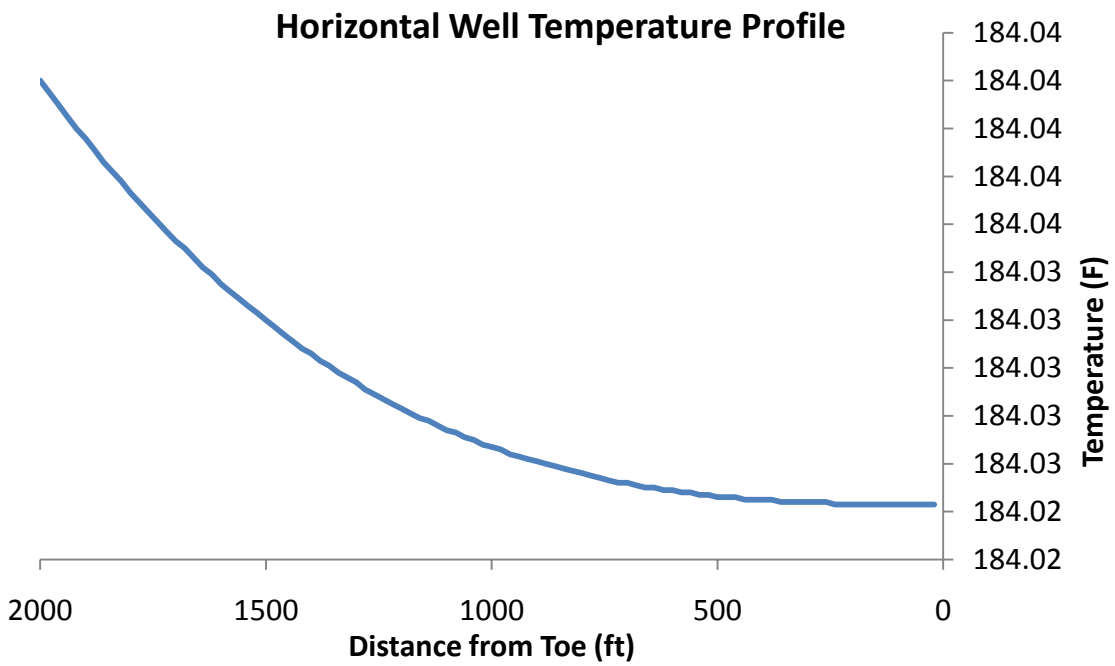

Fig. 5.2: Temperature Profile for a Horizontal Well; 6” in Diameter.

We can see from this run that the temperature of the fluid flowing in the reservoir heated up (4.02 F) arriving at the wellbore at a temperature of (184.02 F). This is the incoming fluid temperature at the toe of the horizontal well which is equal to the wellbore temperature at the toe segment as indicated in our assumptions earlier; please refer to Section 4.3. This heating effect is expected since the Joule-Thompson coefficient, which combines the effect of viscous dissipation and fluid expansion, is negative for the oil and the pressure drop in the reservoir is negative and that results in a rise in the temperature of the fluid as it flows in the reservoir.

Fig. 5.1 gives us typical pressure drops in wellbores. This case with 8,565 BPD, we observe a pressure drop of only (1.93) psi. Moreover, the plot shows the effect of inflow on the pressure drop. As we can see, the pressure drop increases as we go towards the heel. That is because more fluid is entering the wellbore and the inflow rates increase the friction factor, the mass in the system and the velocity.

Fig 5.2 also shows a typical increase in temperature in the wellbore. This slight increase is a result of the small pressure drop experienced in the wellbore. The wellbore is (6 inches) in diameter which is considered large. Typical wellbore diameters for horizontal wells vary somewhere between (2.5 inches – 4 inches). Six inches diameter is common with multilateral wells and this is the reason for our selection.

Fig. 5.3 and **Fig. 5.4** show the results of the pressure and temperature profile for a case similar to the previous one but with the wellbore diameter reduced to four inches. The total rate is 8,558 BPD and the pressure drop along the lateral increases to 14.1 psi and the temperature rise across the wellbore is 0.13 F. The higher pressure drop is

caused by the fact that the wellbore is smaller. The higher pressure drop caused the temperature rise to be higher.

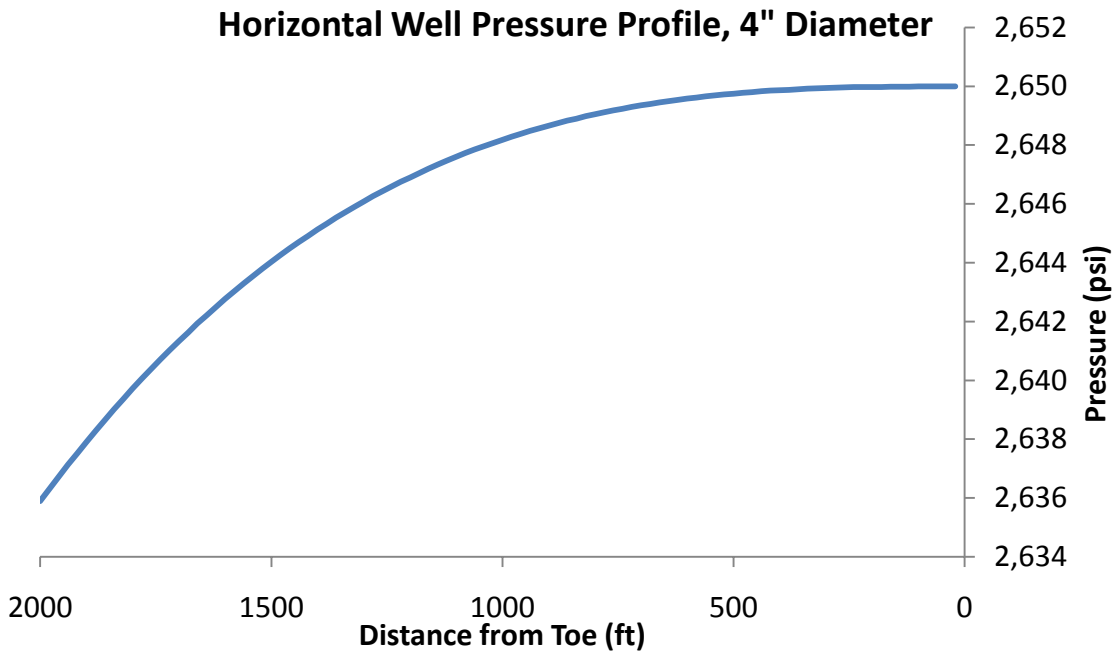

Fig. 5.3: Pressure Profile for a Horizontal Well; 4" in Diameter.

To understand the difference in pressure and temperature profiles when a different phase is flowing, we will compare simulation runs for single phase oil and single phase water. That is, we conduct three runs assuming that only the oil phase exists and we vary the drawdown pressure. After that, we conduct the same runs but assuming that only the water phase exists. The similarity will be in all geometrical aspects of wellbore and reservoir as well as the pressure drawdown. Properties used for the water are summarized in Table 5.4. The results of these runs are summarized in Table 5.5. The Table shows that for both oil and water, the arriving inflow temperature is higher than the geothermal temperature, which is 180 F, and that the fluid heats up in the wellbore as

a result of the pressure drop. However, it can be seen in Table 5.5 that the heating experienced in the reservoir and in the wellbore is higher for the oil phase. That is mainly because the Joule-Thompson coefficient for oil is higher than that for the water. **Fig. 5.5** and **Fig. 5.6** show the pressure and temperature profiles for the oil and water phases. ΔT and ΔP represent the temperature and pressure change across the horizontal well.

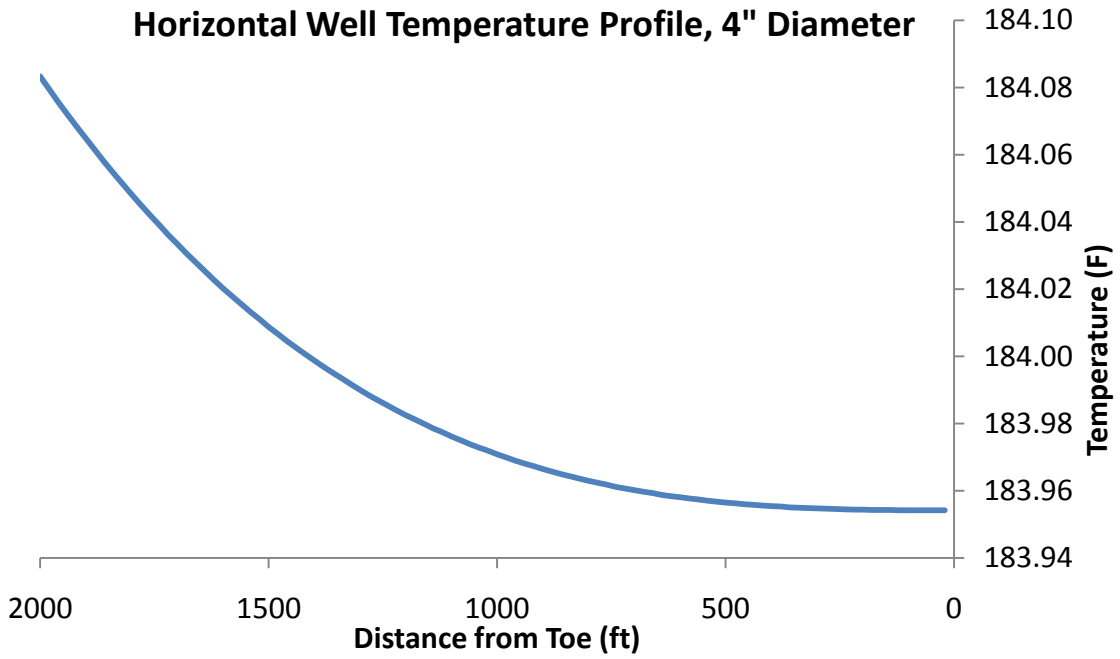

Fig. 5.4: Temperature Profile for a Horizontal Well; 4" in Diameter.

Table 5.4: Fluid Properties Used for Water.

Viscosity (cP)	0.48
Density (Ib_m/ft^3)	63.04
Specific Heat Capacity (Btu/Ib_m-F)	1.002
Thermal Expansion Coefficient (1/F)	0.000311
Conductivity (Btu/hr-ft-F)	2.5

Table 5.5: Summary of Oil and Water Runs at Different Drawdown Pressures.

Phase	Drawdown Pressure (psi)	Diameter (in)	T_{in} (F)	ΔT (F)	ΔP (psi
Oil	300	6	188.14	0.07	-7.7
Oil	200	6	185.40	0.03	-3.4
Oil	100	6	182.65	0.01	-0.9
Water	300	6	183.16	0.10	-28.6
Water	200	6	182.08	0.05	-12.6
Water	100	6	181.01	0.01	-3.14

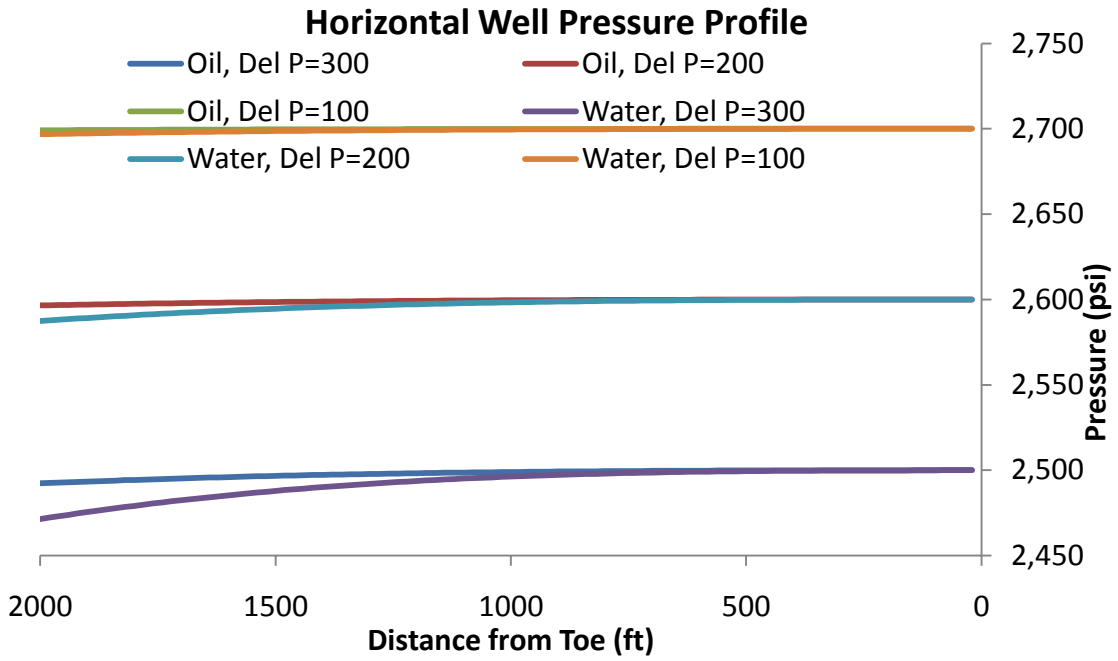

Fig. 5.5: Pressure Profiles in the Wellbore for Oil and Water Cases, 4" Diameter.

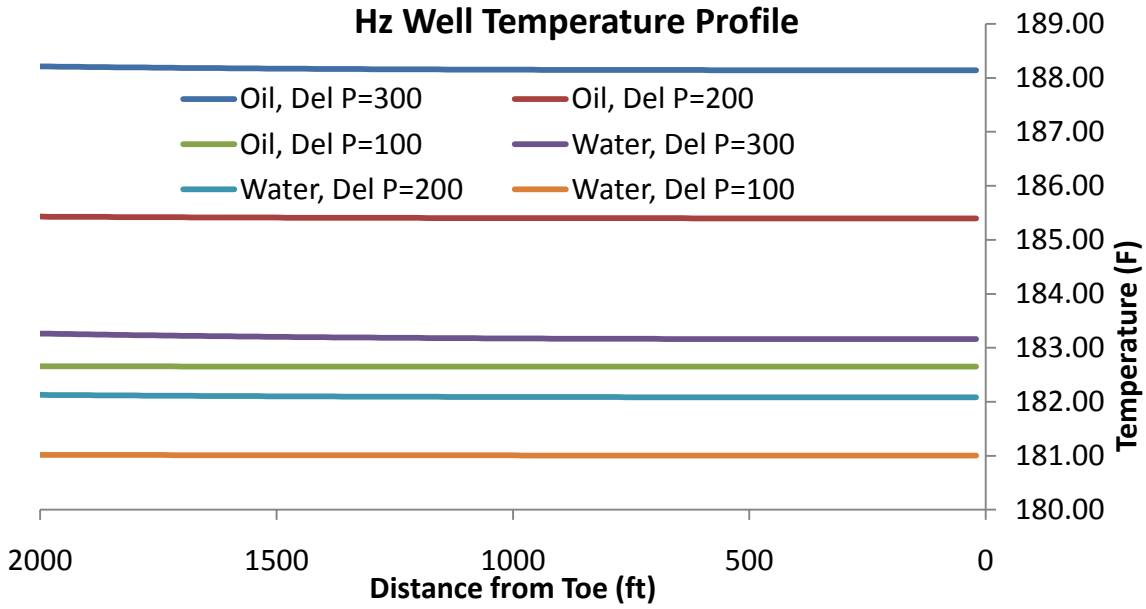

Fig. 5.6: Temperature Profiles for a Horizontal Well for Oil and Water Flow, 4" Diameter.

5.2 Results for Multilateral Wells

Now that we have formulated a good understanding for some horizontal well cases, we turn to our analysis which covers the case of single phase oil flow and two-phase oil and water flow. The oil and water properties are shown by Table 5.2 and Table 5.4. Our base case is a trilateral well in which all three laterals are identical and produce oil. The properties of each lateral are presented in Table 5.1 and other important parameters for the motherbore are shown in Table 5.6. For all the multilateral well runs, we keep the pressure at the heel at 2,650 psi as indicated in Table 5.6.

Table 5.6: Key Parameters for the Motherbore, Base Case.

D (in)	6	Segment with Junction for L2	40
Roughness	0.01	Segment with Junction for L3	60
L (ft)	1000	Total # of Segment	100
Angle (degrees)	0		
P @ Heel (psi)	2650		

We are interested in the pressure and temperature profiles but more specifically in the temperature profile in the motherbore. That is because in multilateral wells, the fiber-optic cable can only be installed in the motherbore. Moreover and up to date, only the temperature can be measured using the DTS technology. Pressure measurement is obtained using pressure sensors that are normally installed below or above the packers in multilateral wells or above the upper packer to obtain one downhole pressure

measurement. Nonetheless, we will still show the results for the pressure profile as if it were continuously measured like temperature.

We want to analyze the change in the temperature and pressure profiles at the segments where the laterals connect to the motherbore. Any temperature change in the order of (0.01 F) or higher is considered detectable and any pressure change in the order of (1 psi) or higher is considered detectable. To obtain this change, we will calculate the difference in temperature and pressure in the segment where the lateral connects, the junction point, and the segment before it. We introduce two variables Del T and Del P so that the change in temperature, Del T, at the segment where lateral #2, L2, connects is the temperature at segment #40 minus the temperature at segment #39. Similarly, the change in temperature, Del T, at the segment where lateral #3, L3, connects is the temperature at segment #60 minus the temperature at segment #59. The same definition applies for Del P. The expressions for Del T and Del P are shown by Eq. 5.1 through Eq. 5.4

$$Del\ T_{Jun\#1} = T_{segmnt\#40} - T_{segmnt\#39} \quad \ldots\ldots (5.1)$$

$$Del\ T_{Jun\#2} = T_{segmnt\#60} - T_{segmnt\#59} \quad \ldots\ldots (5.2)$$

$$Del\ P_{Jun\#1} = P_{segmnt\#40} - P_{segmnt\#39} \quad \ldots\ldots (5.3)$$

$$Del\ P_{Jun\#2} = P_{segmnt\#60} - P_{segmnt\#59} \quad \ldots\ldots (5.4)$$

Table 5.7 summarizes the important results for our base case and **Fig. 5.7** and **Fig. 5.8** show the pressure and temperature profiles in the motherbore.

Table 5.7: Results for the Base Case for Motherbore.

Lateral #1 Oil Rate (BPD)	7,760	Del $T_{Jun\#1}$	0.002
Lateral #2 Oil Rate (BPD)	7,809	Del $P_{Jun\#1}$	-0.02
Lateral #3 Oil Rate (BPD)	7,917	Del $T_{Jun\#2}$	0.01
Motherbore Oil Rate (BPD)	23,486	Del $P_{Jun\#2}$	-0.09
ΔT Across Motherbore (F)	0.08		
ΔP Across Motherbore (psi)	-11.33		

As we alluded to earlier, “Del T” and “Del P” represent the temperature and pressure change at the segments where the laterals connect to the motherbore. That is the reason we do not calculate the value for these two parameters at the segment where lateral #1, L1, enters because it is the start of the motherbore and no segment precedes it.

Table 5.7 shows that in this case, neither the pressure nor the temperature change in the motherbore is in the detectable range except at L3, segment #60, where the change in temperature barely met our criteria. Therefore, when all the laterals are identical, no distinct signature is seen on either the pressure or temperature profile.

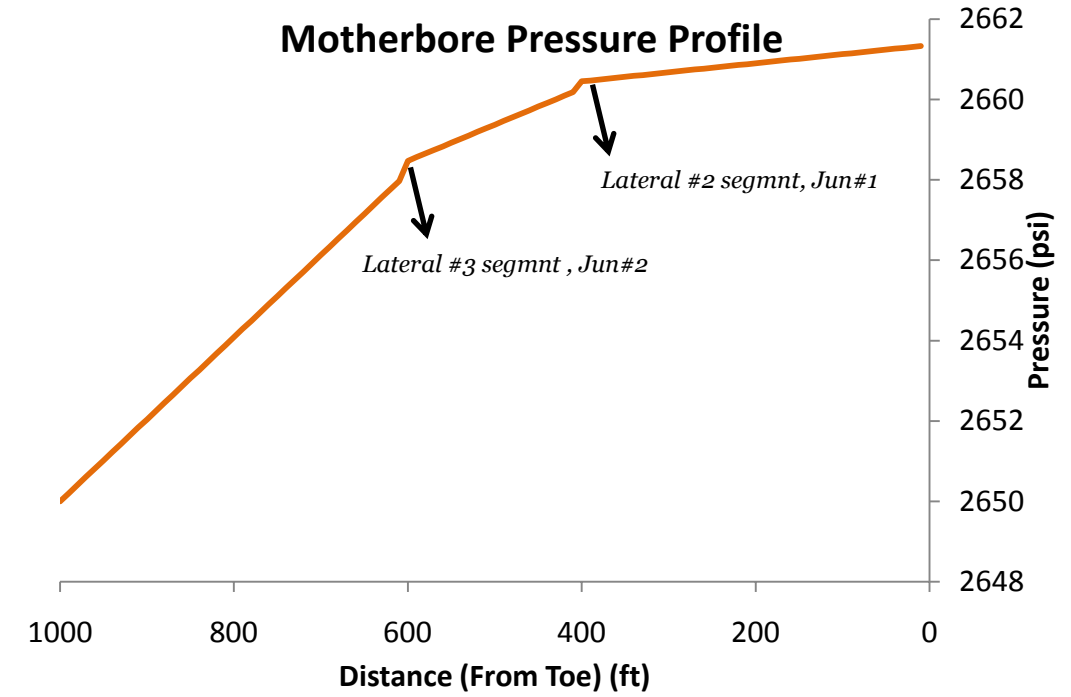

Fig. 5.7: The Pressure Profile in the Motherbore, Base Case.

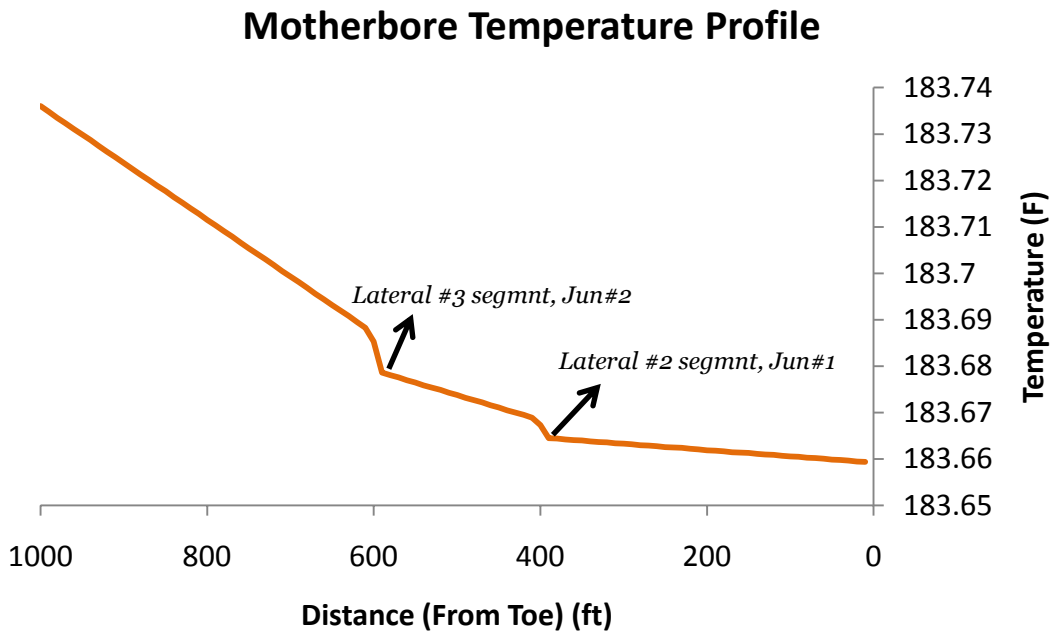

Fig. 5.8: The Temperature Profile in the Motherbore, Base Case.

It is noteworthy to highlight the change of the slope of the pressure and temperature profiles shown on Fig. 5.7 and Fig. 5.8. The points where the slope changes correspond to junction segments or segments where laterals connect to the motherbore. For the pressure profile plot, the slope increases which indicates that the pressure gradient increases. That is caused by the fact that more fluid is entering at these junction points increasing the mass and velocity in the system. This increase in mass and velocity causes an increase in the pressure drop as more fluid enters the motherbore from the lateral. The increase in pressure drop gradient after each junction point causes an increase in the temperature gradient. Therefore, we see both the pressure and temperature gradients increase after each junction point.

In field applications, the interest is normally to identify which lateral or laterals are damaged or are producing water if water cut is detected on the surface. To investigate these issues, we will study the effect of varying three different parameters on the pressure and temperature profiles. Namely, we will vary the permeability, length and the water cut produced in one of the laterals and study the effect on the pressure and temperature profiles. In this work, unless otherwise indicated, we choose lateral #2, L2, and to its permeability, length and produced water cut. Table 5.8 shows a description of the different runs made that will be referred to in the following discussion.

Table 5.8: Description of the Simulation Runs.

Run #	Description
1	Base case; all lateral are identical. Please refer to Table 5.1, 5.2 and 5.6
2	Similar to run#1, permeability of L2 is 55 mD
3	Similar to run#1, permeability of L2 is 45 mD
4	Similar to run#1, permeability of L2 is 32 mD
5	Similar to run#1, permeability of L2 is 10 mD
6	Similar to run#1, length for L2 is 1500’
7	Similar to run#1, length for L2 is 1000’
8	Similar to run#1, length for L2 is 500’
9	Similar to run#1, water produced from L2 and water cut=12%
10	Similar to run#1, water produced from L2 and water cut=23%
11	Similar to run#1, water produced from L2 and water cut=32%
12	Similar to run#1, water produced from L2 and water cut=42%

As shown by Table 5.8, we start by reducing the permeability in L2 and analyzing the effect on the pressure and temperature profiles. **Fig. 5.9** and **Fig. 5.10** show the calculated profiles for all the cases considered in which permeability was reduced by 13%, 29%, 49% and 84%. For the first case in which permeability was reduced by 13% (run#2) the pressure profile shows clear breaks at the lateral junction points, the pressure differential at these segments is less than 1 psi. So is considered undetectable. On the other hand, the temperature profile showed a much more dramatic shift at L2 junction with a temperature differential, Del $T_{Jun\#1}$, of (-0.05 F) but a less temperature differential at L3 junction, (0.01 F). So, we can see that the fluid coming from L2 enters the wellbore at a cooler temperature which is a result of the lower flow

rates produced from the lateral. L2 produced around 1700 – 1800 BPD less than the other two laterals which translated into a lower temperature. Based on this finding, we expect the temperature differential to increase as we reduce the permeability in L2 further.

In run#3, the permeability in L2 is reduced 29% and the pressure change at segments #40 and #60 was less than 1 psi and so is undetectable. However, the temperature profile shows a sharp jump at the junction of L2 with a temperature change, Del $T_{Jun\#1}$, of -0.1 F and a temperature change at the junction of L3 equal 0.02 F. The rate produced from L2 is less in this run than was in run#2 resulting in a lower fluid temperature for the fluid coming from L2. This shows up as a sharp jump in the temperature profile at L2 junction. Also in this run, a better temperature change is observed at the junction of L3. That is because the fluid in motherbore is cooled down by the fluid from L2 more in this run compared to the previous run.

The same trend continues in run#4 and run#5. Fig. 5.10 shows clearly that as the permeability is reduced further in L2, less fluid is produced, resulting in a less heating effect. As the cooler fluid from L2 enters the motherbore, a higher temperature change is observed at both junction points for both lateral #2 and lateral #3. Also, we can see that the temperature change or differential is always higher at junction of L2 than it is at the junction of L3. Table 5.9 summarizes the results for simulation runs in which permeability of L2 was varied.

Table 5.9: Key Results for Simulation Runs where Permeability is Varied.

Run #	% Perm. Reduction	L1, Qo (BPD)	L2			L3		
			Qo, BPD	Del $T_{Jun\#1}$ (F)	Del $P_{Jun\#1}$ (psi)	Qo, BPD	Del $T_{Jun\#2}$ (F)	Del $P_{Jun\#2}$ (psi)
2	-13	7,839	6,134	-0.05	-0.02	7,075	0.01	-0.07
3	-29	7,919	4,305	-0.10	-0.02	8,035	0.02	-0.06
4	-49	7,998	2,292	-0.14	-0.02	8,095	0.02	-0.04
5	-84	8,070	252	-0.27	-0.02	8,151	0.04	-0.03

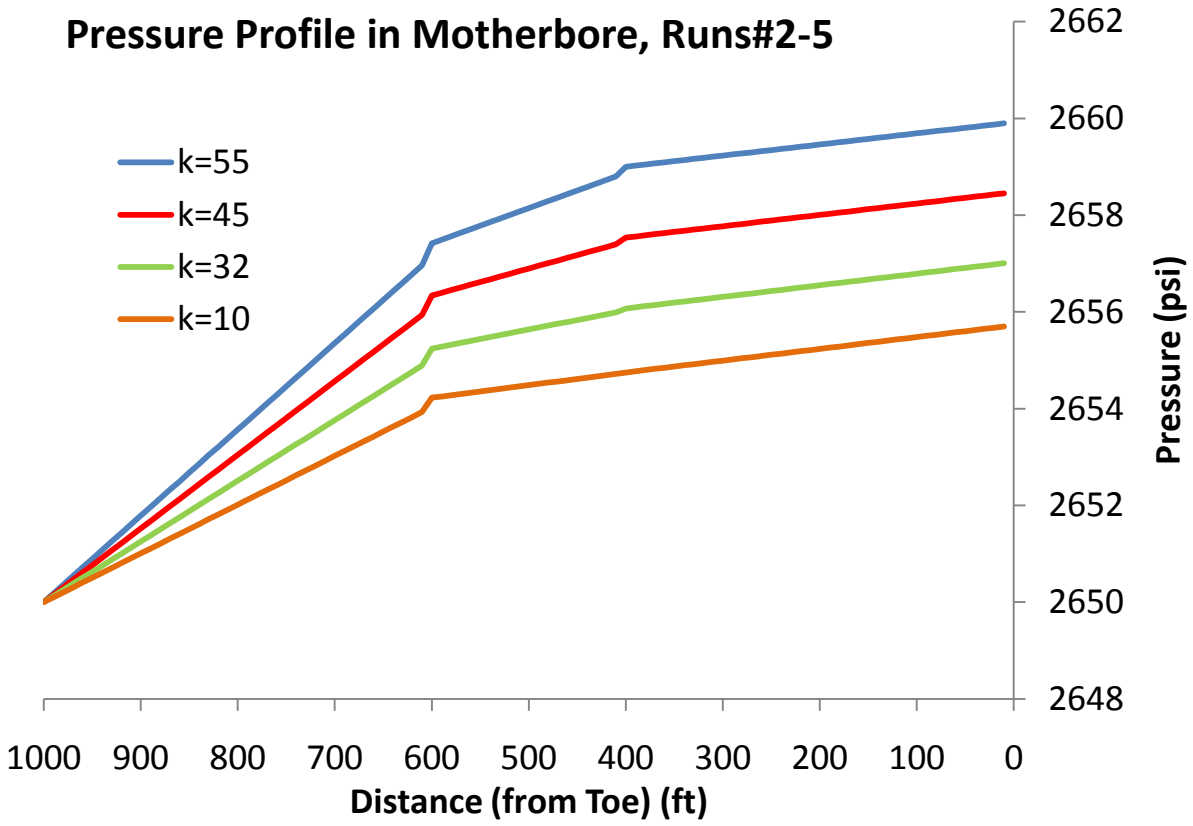

Fig. 5.9: Pressure Profiles for Cases where Permeability of L2 was Reduced.

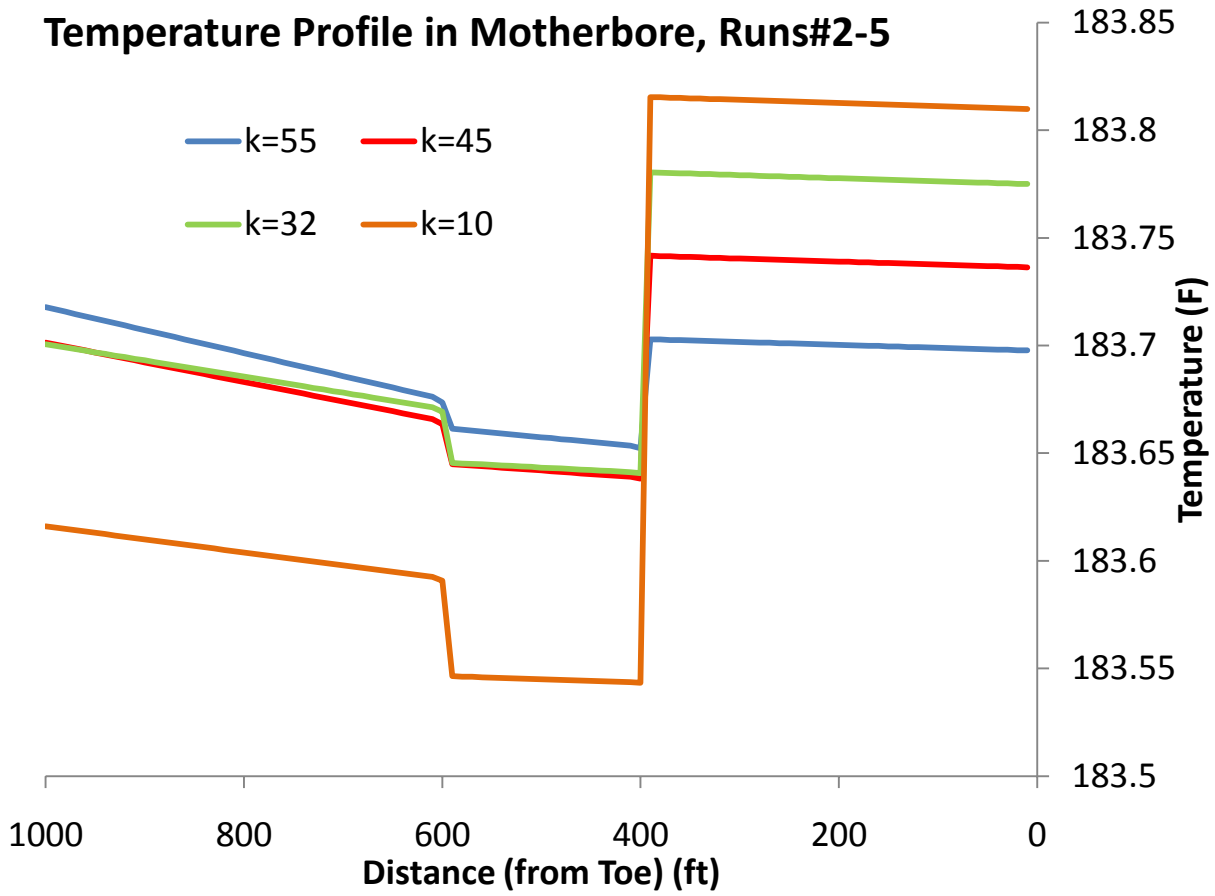

Fig 5.10: Temperature Profiles for Cases where Permeability of L2 was Reduced.

Now that we have analyzed the effect of permeability reduction, we move to altering the length of L2 and studying its effect on the pressure and temperature profiles; Table 5.8 gives the description of each run. **Fig. 5.11 and Fig. 5.12** show the pressure and temperature profiles for these cases. In the first of these runs, run#6, we reduce the length by 25% to 1500'. The results show the reducing the length by 25% while keeping everything else the same does not result in a detectable temperature and pressure change in the junction points. The temperature change at segments #40, "Del $T_{Jun\#1}$", and at segment #60, "Del $T_{Jun\#2}$", was barely 0.01 F. Also, the pressure differential at both segments, Del $P_{Jun\#1}$ and Del $P_{Jun\#2}$, was less than 1 psi. The same results are found when the length in L2 is reduced by 50% and 75% as summarized by Table 5.10. This shows that varying the length of L2 does not have a significant effect on the temperature profile at the junction points.

To further understand these results, we analyze the temperature profiles for L2 in all the three runs where we varied the length. As a reminder, we have noted in our model that T_{in} stands for the incoming or inflow temperature which is the reservoir temperature at a distance equal to the wellbore radius, r_w. We can see that decreasing the length had the effect of increasing the incoming fluid temperature from the reservoir or T_{in} in our model. However, this increase was not significant enough and therefore the fluid coming from L2 did not show a distinct signature on the motherbore temperature profile. However for cases in which we varied permeability, the net effect of reducing permeability is reducing the incoming inflow temperature causing the temperature change at L2 junction, Del $T_{Jun\#1}$, to get larger. Table 5.11 shows the results for the

inflow temperatures in L2, T_{in}, as we change permeability and length. Since we can evaluate T_{in} for each segment, we have chosen to show T_{in} for first segment, or toe segment.

Table 5.10: Key Results for Simulation Runs where Length is Varied.

Run #	% Length Reduction	L1, Qo (BPD)	L2			L3		
			Qo, BPD	Del $T_{Jun\#1}$ (F)	Del $P_{Jun\#1}$ (psi)	Qo, BPD	Del $T_{Jun\#2}$ (F)	Del $P_{Jun\#2}$ (psi)
6	-25	7,846	5,973	0.01	-0.02	7,981	0.01	-0.07
7	-50	7,929	4,046	0.01	-0.02	8,043	0.01	-0.05
8	-75	8,007	2,049	0.01	-0.02	8,102	0.00	-0.04

Table 5.11: Inflow Temperatures for L2 for Runs#2-8.

Run #	Inflow Temperature, T_{in} (F)	Parameter Changed
2	183.31	Permeability reduced 13%
3	182.82	Permeability reduced 29%
4	182.08	Permeability reduced 49%
5	180.53	Permeability reduced 84%
6	183.74	Length reduced 25%
7	183.81	Length reduced 50%
8	183.86	Length reduced 75%

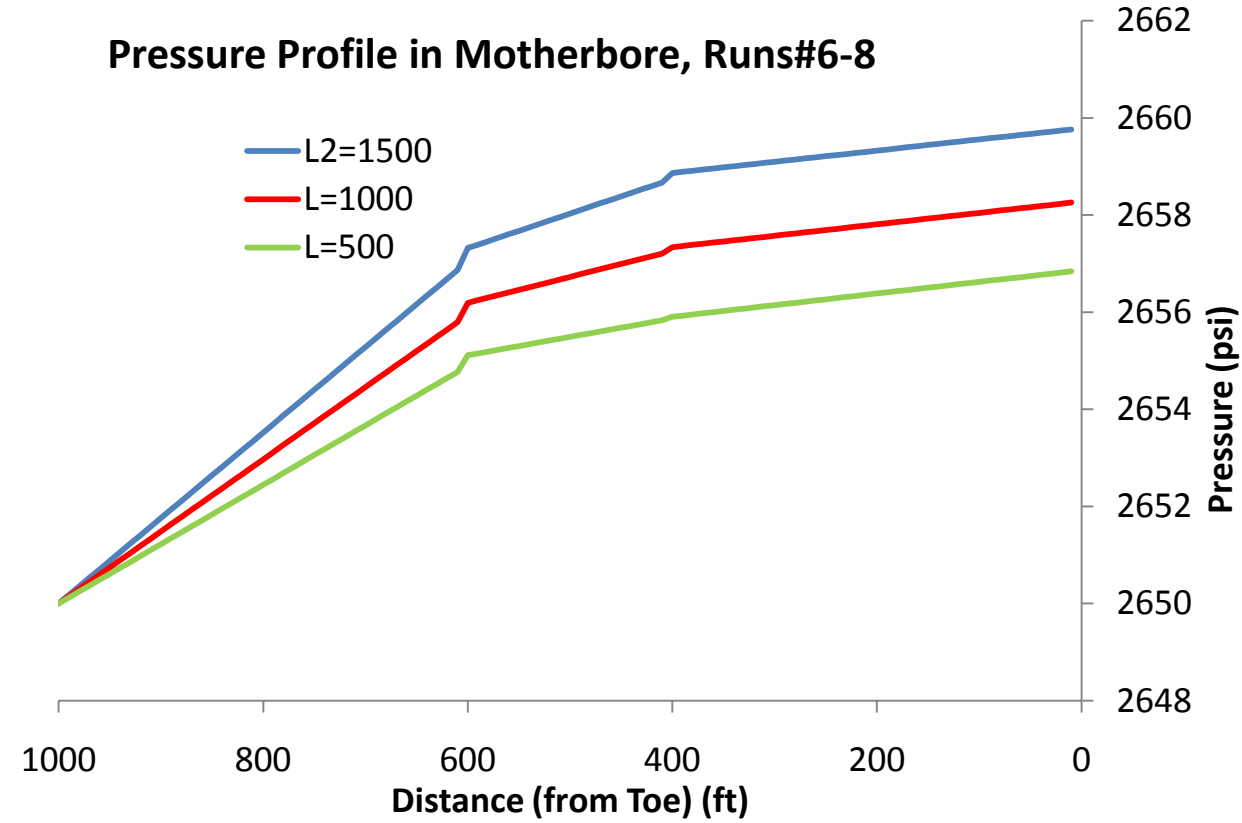

Fig. 5.11: Pressure Profiles in the Motherbore; Cases where the Length was Varied.

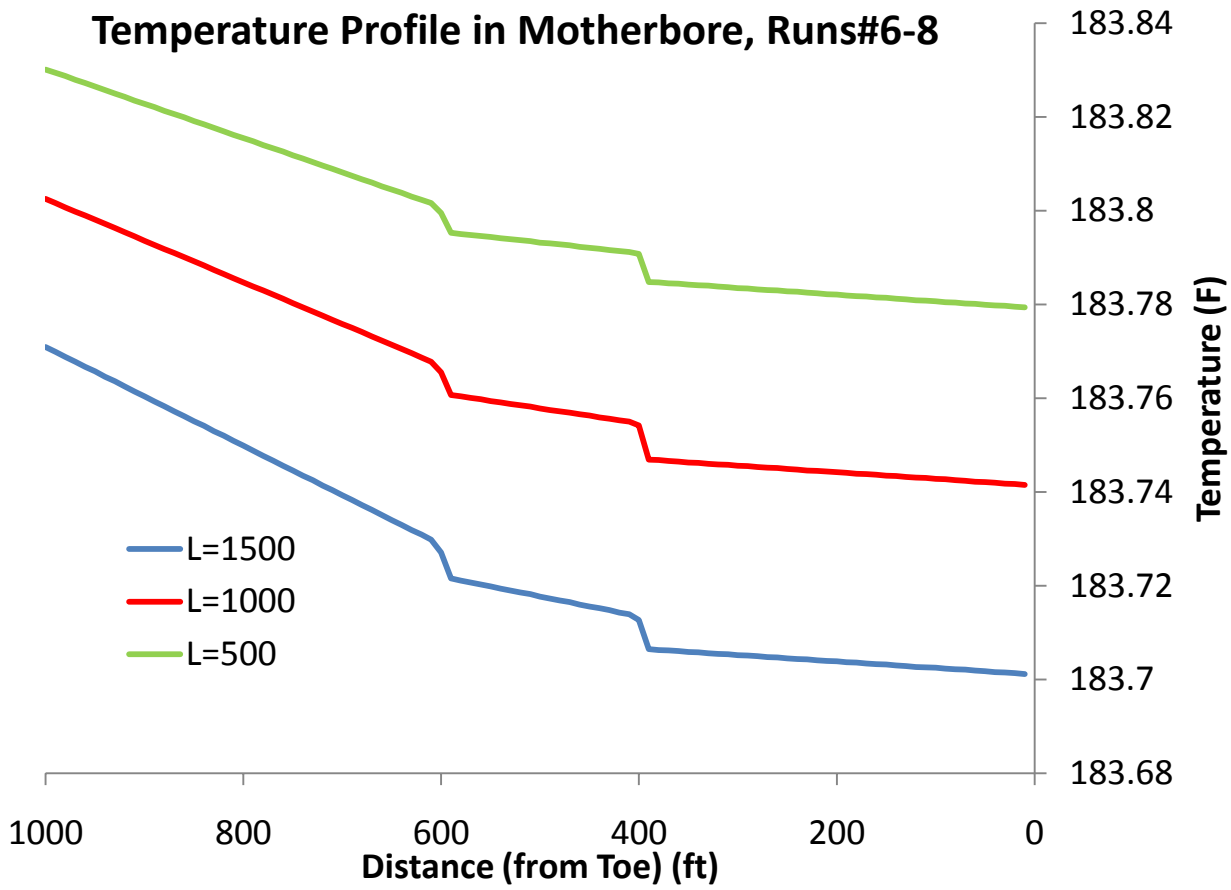

Fig. 5.12: Temperature Profiles in the Motherbore; Cases where the Length was Varied.

Now we analyze another common scenario in which L2 produces water. To understand the effect of water production, we will vary the water cut as shown by Table 5.8. It is worth mentioning that the water cut is calculated as the total water produced from the well divided by the total liquid production. We recall from our analysis for horizontal wells and as was noted by Dawkrajai (2006) and Yoshioka (2007) that water causes less heating effect than oil. Therefore, we expect the temperature of the fluid coming from L2 to get cooler as the water cut increases.

Fig. 5.13 and **Fig. 5.14** show the pressure and temperature profiles for the runs in which the water cut was varied in L2. For the case when the water cut is 12%, the pressure differential at the lateral junctions was not significant but the temperature differential, Del $T_{Jun\#1}$, at the junction for L2 is (-0.45 F) and for L3 is (0.11 F). These changes can be easily detected with the DTS technology. We also note that the fluid from L2 enters the wellbore at a cooler temperature as we expected since water does not heat up the reservoir and the wellbore as the oil does. Table 5.12 summarizes the key results for runs where the water cut is varied.

Table 5.12: Key Results for Simulation Runs where Water Cut is Varied.

Run #	WC %	L1, Qo (BPD)	L2				L3		
			Qo, BPD	Qw, BPD	Del $T_{Jun\#1}$ (F)	Del $P_{Jun\#1}$ (psi)	Qo, BPD	Del $T_{Jun\#2}$ (F)	Del $P_{Jun\#2}$ (psi)
9	12	7,680	5,724	2,997	-0.45	-0.02	7,859	0.11	-0.11
10	23	7,597	3,861	5,790	-0.66	-0.02	7,798	0.15	-0.13
11	32	7,522	2,264	8,194	-0.75	-0.02	7,744	0.16	-0.15
12	42	7,419	227	11,296	-0.80	-0.02	7,671	0.14	-0.17

As we can see from Table 5.11, as water cut increases, the fluid from L2 comes into the motherbore at cooler temperature which results in a higher temperature differential at that junction. The temperature differential values shown in Table 5.11 are well within the detectable range for DTS technology. Also, the temperature differential at L3 junction is also high when compared to all previous cases in this study. The reason is that the cooler fluid from L2 cools the motherbore and when the fluid reaches the junction for L3, it encounters a hotter fluid and that causes the temperature differential to be higher.

All the calculations so far assumed six inches diameter for all the laterals and the motherbore. We know that reducing the diameter has the effect of increasing the pressure drop which in turn increases the temperature in the wellbore. So to study the effect of reducing the diameter, we choose the next most common completion tubing size for multilateral wells which is four inches. After that, we perform all the runs shown by Table 5.8 and analyze the resulting pressure and temperature profiles. The results are

summarized in Table 5.13, Table 5.14 and Table 5.15. The results show that we basically reach the same conclusions as with the 6-inch diameter cases.

Table 5.13: Key Results for Simulation Runs where Permeability is Varied, 4" Diameter.

Run #	% Perm. Reduction	L1, Qo (BPD)	L2			L3		
			Qo, BPD	Del $T_{Jun\#1}$ (F)	Del $P_{Jun\#1}$ (psi)	Qo, BPD	Del $T_{Jun\#2}$ (F)	Del $P_{Jun\#2}$ (psi)
2	-13	5,722	4,662	-0.03	-0.09	6,228	0.03	-0.30
3	-29	5,934	3,414	-0.07	-0.10	6,389	0.03	-0.25
4	-49	6,175	1,901	-0.10	-0.11	6,576	0.04	-0.19
5	-84	6,422	219	-0.40	-0.12	6,774	0.08	-0.13

Table 5.14: Key Results for Simulation Runs where Length is Varied; 4” Diameter.

Run #	% Length Reduction	L1, Qo (BPD)	L2			L3		
			Qo, BPD	Del $T_{Jun\#1}$ (F)	Del $P_{Jun\#1}$ (psi)	Qo, BPD	Del $T_{Jun\#2}$ (F)	Del P_{Jun2} (psi)
6	-25	5,738	4,568	0.02	-0.09	6,241	0.02	-0.30
7	-50	5,964	3,226	0.02	-0.10	6,413	0.02	-0.24
8	-75	6,206	1,696	0.02	-0.11	6,601	0.02	-0.18

Table 5.15: Key Results for Simulation Runs where Water Cut is Varied; 4” Diameter.

Run #	WC %	L1, Qo (BPD)	L2				L3		
			Qo, BPD	Qw, BPD	Del $T_{Jun\#1}$ (F)	Del $P_{Jun\#1}$ (psi)	Qo, BPD	Del $T_{Jun\#2}$ (F)	Del $P_{Jun\#2}$ (psi)
9	12	5,372	4,060	2,060	-0.31	-0.08	5,968	0.12	-0.40
10	22	5,225	2,684	3,815	-0.46	-0.08	5,861	0.15	-0.45
11	31	5,075	1,355	5,533	-0.53	-0.07	5,752	0.16	-0.49
12	41	4,919	0	7,287	-0.55	-0.07	5,640	0.15	-0.54

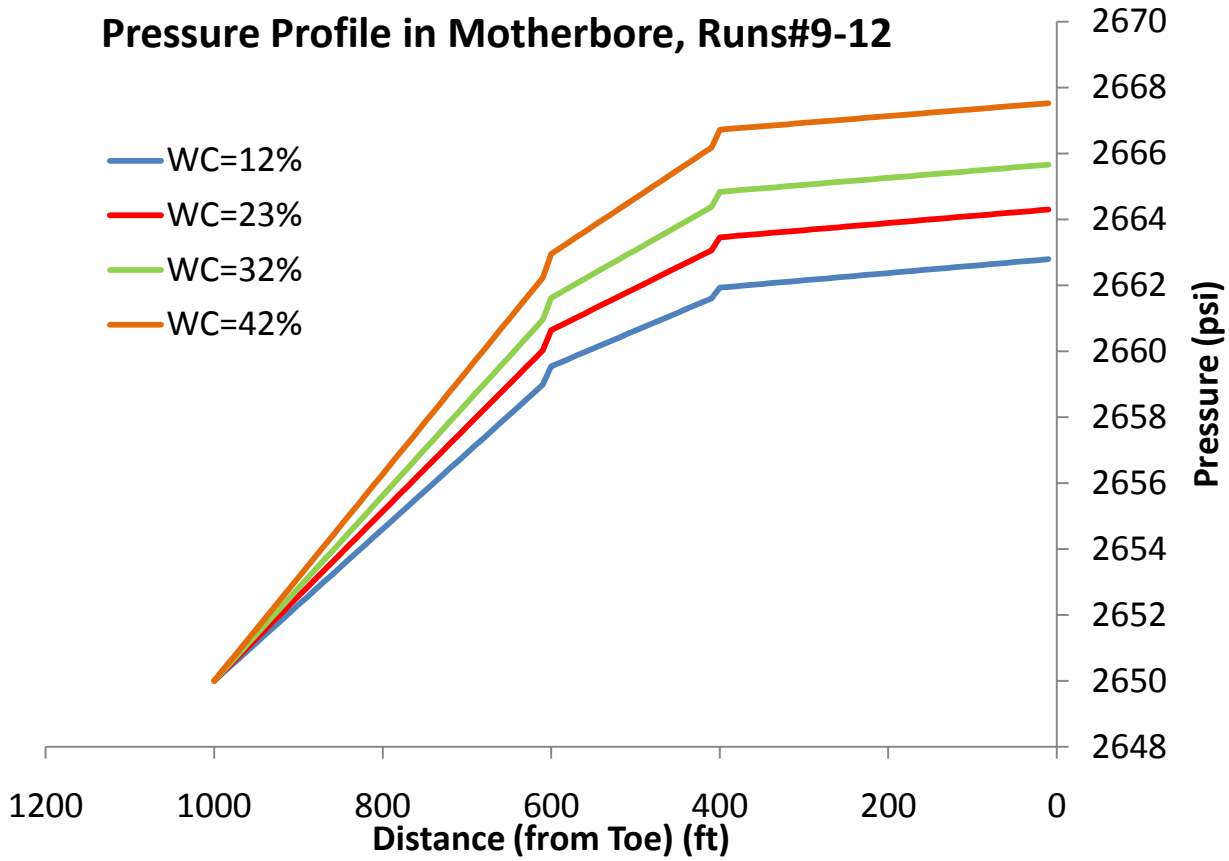

Fig. 5.13: Pressure Profiles in the Motherbore; Cases where the Water Cut was Varied.

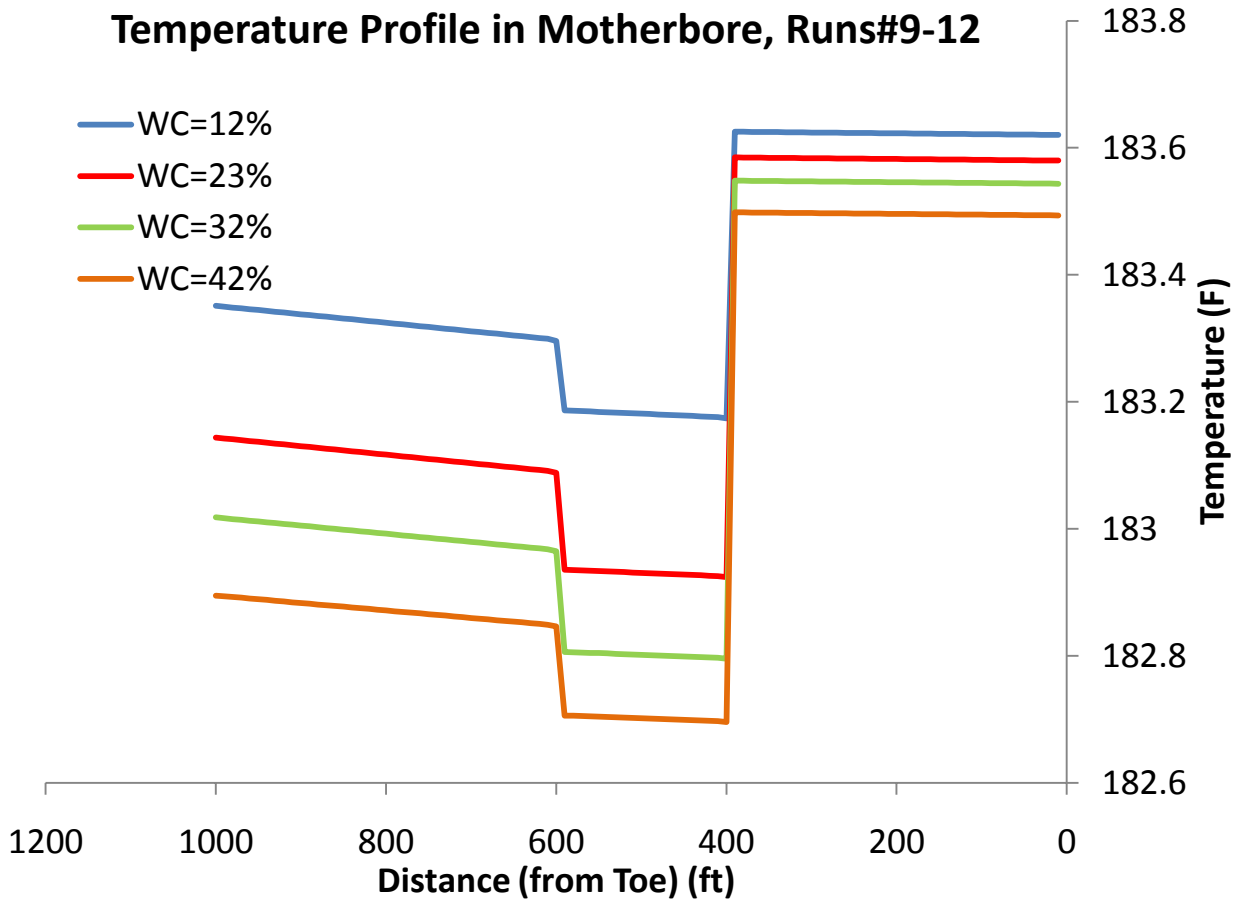

Fig. 5.14: Temperature Profiles in the Motherbore; Cases where the Water Cut was Varied.

6. CONCLUSIONS AND RECOMMENDATIONS

6.1 Conclusions

In this research, we developed a steady-state model to calculate the pressure and temperature profiles in multilateral wells. Drainage areas for all laterals were supplied as input and the only interference between the laterals happens at the junction points in the motherbore. Rock and fluid properties were calculated at average pressure and temperature expected for each simulation run and then were kept constant throughout the simulation run. This assumption is believed to be valid since the temperature and pressure variations are not going to be significant to alter the fluid properties. The model accounted for the pressure drop and the associated temperature change across the inflow control valve, ICV. The pressure drop calculations across the valve were performed using correlations provided by the equipment vendor.

In field applications, the interest is in identifying damaged lateral, the contribution from each lateral or to identify which lateral or laterals are producing water if water is seen on the surface. Therefore to investigate these issues, we varied the permeability, length and water cut in lateral #2, or L2 in our notation, and studied the effect on both the pressure and temperature profiles in the motherbore.

Our results show that reducing the permeability in L2 causes the fluid coming from that lateral to be cooler than the fluid in the motherbore and resulted in a detectable impact on the motherbore temperature profile that can be measured with DTS technology. Also, introducing water in the L2 causes the fluid coming from L2 to be

cooler than the fluid in the motherbore and results in a detectable impact on the temperature profile. On the other hand, reducing the length of L2 does not alter the temperature profile in the motherbore significantly and change cannot be detected with DTS technology. Moreover, the pressure profile in all cases does not show a detectable change at the junction segments which indicates that the pressure data cannot be used to identify damaged laterals or laterals which produce water, if present. The same conclusions are reached whether we use 6-inch or 4-inch diameter wellbores.

6.2 Recommendations

Due to the time limitation, an inversion model was not developed and verification of the model using field data was not possible in this research. Therefore, we recommend developing an inversion model and testing it using field data to establish applicability as well as limitation. Moreover, the reservoir model used assumed constant rock properties and single phase flow in each reservoir segment. Although different segments in the reservoir are allowed to have different permeabilities and different phases, it is better to develop a numerical reservoir model that would relax a lot of the assumptions made in this research. Also, such a model will enable analyzing cases where the water produced either comes from the bottom formations or comes from the injection wells. Moreover, the numerical model will allow interference between the laterals in the reservoir which resembles the reality of multilateral wells.

REFERENCES

Al-Kaabi, A.O. 2008. Haradh-III: Industry's largest Field Development with Maximum Reservoir Contact Wells, Smart-Well Completions and the Ifield Concept. *SPE Production & Operations* **23** (4): 444-447.

Bird, R. B., Stewart, W. E. and Lightfoot, E. N. 2002. *Transport Phenomena*. New York: J. Wily.

Dawkrajai, P. 2006. Temperature Prediction Model for a Producing Horizontal Well. PhD dissertation, University of Texas, Austin, TX.

Furui, K. 2003. A Rigorous Formation Damage Skin Factor and Reservoir Inflow Model for a Horizontal Well. *SPE Production & Facilities* **18** (3): 151-157.

Glasbergen, G., Gualtieri, D., Domelen, M. S., Sierra, J. 2009. Real-Time Fluid Distribution Determination in Matrix Treatments Using DTS. *SPE Production & Operations* **24** (1): 135-146. SPE-107775-PA. DOI: 10.2118/107775-PA

Hembling, D.E., Berberian, G., Carter N. and John, N.G.2008. Enabling Efficient Permanent Production Monitoring of Advanced Well Completions in Saudi Arabia Using Fiber-optic Distributed Temperature Sensing. Paper SPE 115255 presented at the SPE annual Technical Conference and Exhibition, Denver, CO, 21-24 September. DOI:10.2118/115255-MS

Hill, A.D. 1990. *Production logging: Theoretical and Interpretive Elements.* Monograph Series, SPE, Richardson, TX **14**.

Jayawardena, S.S., Alkaya, B., Redus, C.L. and Brill, J.P. 2000. A New Model for Dispersed Multi-Layer Oil-Water Flow. 2nd *North American Conference on Multiphase Technology*, Banff, Canada, **40**: 77-89.

Kim, D. and Ghajar, A.J. 2002. Heat Transfer Measurements and Correlations for Air-Water Flow of Different Flow Patterns in a Horizontal Pipe. *Experimental Thermal and Fluid Science* **25** (8): 659-676.

Mccain, W.D. 1990. *The Properties of Petroleum Fluids*. Tulsa, OK: PennWell Books.

Nath, D.K., Finley, D.B., and Kaura, J.D. 2006. Real-Time Fiber-Optic Distributed Temperature Sensing (DTS): New Applications in the Oilfield. Paper SPE-103069 presented at the SPE Annual Technical Conference and Exhibition, San Antonio, TX, 24-27 September. DOI: 10.2118/103069-MS.

Ouyang, L.B, 1998. Single-Phase and Multiphase Fluid Flow in Horizontal Wells. PhD dissertation, Stanford University, Stanford, CA.

Prats, M. 1982. *Thermal Recovery.* Monograph Series, SPE, Richardson, TX **7**.

Eclipse Technical Manual. 2008. Schlumberger. Houston, TX.

Sensornet Ltd. 2009. http://www.sensornet.co.uk/products-services/upstream-oil-gas/digital-flow-profiling/.

Shi, H., Holmes, J., Durlofsky, L., Aziz, K., Daiz, L., Alkaya, B. and Oddie, G. 2005. Drift-flux Modeling of Two-Phase Flow in Wellbores. *SPE Journal* **10** (1): 24-33. SPE-84228-PA. DOI:10.2118/84228-PA.

Shoham, O. 2006. *Mechanistic Modeling of Gas-Liquid Two-Phase flow in Pipes.* Textbook Series, SPE, Richardson, TX.

Sieder, E.N. 1936. Heat Transfer and Pressure Drop of Liquids in Tubes. *Industrial and Engineering Chemistry* **28**: 1429-1435.

Sui, W. 2009. Determining Multilayer Formation Properties from Transient Temperature and Pressure Measurements. PhD dissertation, Texas A&M University, College Station, TX.

Yoshioka, K. 2007. Detection of Water or Gas Entry into Horizontal Wells by Using Permanent Downhole Monitoring Systems. PhD dissertation, Texas A&M University, College Station, TX.

VITA

Name: Rashad Madees K. Al-Zahrani

Address: Harold Vance Department of Petroleum Engineering

Texas A&M University

3116 TAMU – 507 Richardson Building

College Station, TX 77843-3116

Email Address Rashad.zahrani@aramco.com

rashadmalzahrani@gmail.com

Education: B.S., Petroleum Engineering, University of Kansas, 2005.

M.S., Petroleum Engineering, Texas A&M University, 2011